Controlled thermal oxidative crosslinking of polymers of intrinsic microporosity towards tunable molecular sieve membranes.

AUTHOR(S):

Song, Qilei; Cao, Shuai; Pritchard, Robyn H; Ghalei, Behnam; Al-Muhtaseb, Shaheen A; Terentjev, Eugene M; Cheetham, Anthony K; Sivaniah, Easan

CITATION:

Song, Qilei ...[et al]. Controlled thermal oxidative crosslinking of polymers of intrinsic microporosity towards tunable molecular sieve membranes.. Nature communications 2014, 5: -4813: 4813.

ISSUE DATE:

2014-09-04

URL:

http://hdl.handle.net/2433/191074

Controlled thermal oxidative crosslinking of polymers of intrinsic microporosity toward tunable molecular sieve membranes

Qilei Song[1,4], Shuai Cao[2], Robyn H. Pritchard[1], Behnam Ghalei[3], Shaheen A. Al-Muhtaseb[5], Eugene M. Terentjev[1], Anthony K. Cheetham[2], and Easan Sivaniah[1,3]*

[1]Cavendish Laboratory, Department of Physics, University of Cambridge, Cambridge CB3 0HE, UK.
[2]Department of Materials Science and Metallurgy, University of Cambridge, Cambridge CB3 0FS, UK.
[3]Institute for Integrated Cell-Material Sciences (iCeMS), Kyoto University, Kyoto 606-8501, Japan.
[4]Department of Chemical Engineering, Imperial College London, London SW7 2AZ, UK
[5]Department of Chemical Engineering, Qatar University, P.O. Box 2713, Doha, Qatar.
*Correspondence and requests for materials should be addressed to E.S. Email: esivaniah@icems.kyoto-u.ac.jp

Organic open frameworks with well-defined micropore (pore dimensions below 2 nm) structure are attractive next-generation materials for gas sorption, storage, catalysis, and molecular-level separations. Polymers of intrinsic microporosity represent a paradigm shift in conceptualizing molecular sieves from conventional ordered frameworks to disordered frameworks with heterogeneous distributions of microporosity. Polymers of intrinsic microporosity contain interconnected regions of micropores with high gas permeability but with a level of heterogeneity that compromises their molecular selectivity. Here we report controllable thermal oxidative crosslinking of polymers of intrinsic microporosity by heat treatment in the presence of trace amounts of oxygen. The resulting covalently crosslinked networks are thermally and chemically stable, mechanically flexible, and have remarkable selectivity at permeability that is three orders of magnitude higher than commercial polymeric membranes. This study demonstrates that controlled thermochemical reactions can delicately tune the topological structure of channels and pores within microporous polymers and their molecular sieving properties.

Microporous materials with well-defined size-selective channels and pores are promising next-generation molecular sieving materials for gas sorption, storage, and separations[1-3]. Inorganic and organic ordered open frameworks, such as zeolites[4-7], and metal-organic frameworks (MOFs)[8-10], are representative microporous molecular sieving materials with precisely defined pore architecture. Owing to tailored pore size, chemical functionality, and high surface area, these ordered frameworks are promising for gas sorption[8-10], storage[11], catalysis[12], adsorption-based separations[13], and potentially have excellent intrinsic selectivity and permeability in membrane separations[6-7]. However, these

crystalline frameworks are generally brittle and suffer from difficulty in manufacturing to large scale separation membranes[14]. In contrast, industrial selective membranes are made of solution-processable densely packed polymers where molecular transport follows a *solution-diffusion* mechanism, and presents a trade-off between permeability and selectivity[15], known as an upper bound[16-17], as shown in an overview figure (Fig. 1g). Solution-processable and microporous molecular sieving materials are desirable for the next-generation high-performance membranes to achieve both high permeability and high selectivity.

Microporous polymers are a relatively new class of materials that are attractive for applications as organic molecular sieves[18-21]. Polymers of Intrinsic Microporosity (PIMs) [20-27], invented by Budd and McKeown, are a novel sub-class of microporous polymers with unique rigid and contorted macromolecular backbone structure (for example, PIM-1 in Fig. 1a, chemical structure is given in the Supplementary Fig. 1). The poor molecular packing of such rigid chains results in disordered heterogeneous material with regions of irregularly shaped free volume at molecular dimensions in the solid state, as visualized by the molecular simulation (Fig. 1b). The fractional free volume in PIMs is sufficiently high that free volume elements are effectively interconnected, behaving like micropores (pore dimensions below 2 nm) according to the definition of IUPAC. Such high free volume allows the high solubility of gas molecules, while the bottleneck or gates interconnecting micropores behave as sieves for gas molecules with different size and shape. Such interconnected microporosity is analogous to the pore structure of ordered molecular sieves (for example, zeolites), as schematically illustrated in Fig. 1 h. The structure of the interconnected cavities in PIMs materials are also thought to resemble the hour-glass shaped channel systems in naturally occurring biological membranes, such as water channels (known as Aquaporin)[28], and ion channels[29]. Cell membranes utilize such unique channels for rapid molecular and ion transport while providing a chemically gated selection mechanism. Similarly, the unique micropore structure of PIMs materials offers remarkable combinations of permeability and selectivity that surpass the upper bound of synthetic polymer membranes.

In contrast to crystalline molecular sieves, microporous polymers are generally amorphous and flexible. Linear polymer chains interacting by relatively weak van der Waals forces or entanglements could easily slide over each other. In addition, molecular modeling of PIM-1 indicates that spirobisindane (SBI) unit and dioxane linkages are relatively flexible [30]. This amorphous and flexible nature of PIMs polymer chains results in a broad size distribution of free volume elements (e.g. 4 to 10 Å) which compromises their separation performance, for example, poor molecular selectivity, physical aging and plasticization. As indicated by theoretical prediction by Freeman[15], there are two strategies to enhance both the permeability and selectivity of polymeric membrane materials. One approach is improving the solubility selectivity (S_A/S_B), such as PIMs substituted with CO_2-philic tetrazole groups (TZ-PIMs)[20]. An alternative approach is increasing the rigidity of polymer chains while maintaining large interchain spacing, such as thermal rearranged (TR) polymers[18,31], and PIMs with more rigid backbone[21,32-34], for example, PIMs containing rigid Troger's Base (TB) units[21], and triptycene-based PIMs[33-34]. In particular, for separations of industrially and environmentally important gases, such as condensable CO_2 and hydrocarbons in natural gas, all of the existing PIMs polymers have only shown modest selectivity (for example, selectivity of CO_2/CH_4 ~10). Therefore, tailoring the distribution, size, and architecture of channels and pores is critical to achieve a substantial increase of selectivity.

A typical feature of polymers, as soft materials, is their deformability under external stimulus (e.g. light, heat, oxidant, and stress, etc), and even very mild deformation would induce significant change of physical properties. Recently, we reported the photo-oxidative degradation of PIM-1 polymer upon exposure to ultraviolet (UV) light irradiation in the presence of oxygen, which induces oxidative chain scission and local densification at the surface[35]. Similarly, thermo-oxidative degradation or crosslinking could occur for PIM-1 polymer when polymers are heated in the presence of oxygen. The oxidative degradations of conventional polymers are well known, but very limited studies on PIMs polymer materials have been reported. An earlier paper by Li et al. of the Chung group described thermal processing of PIM-1 at 300°C over a period of 1-2 days and reported the simultaneous increase of both permeability *and* selectivity[36]. The work by Li et al. was described as being done within a vacuum oven with no information on the environment in terms of pressure or O_2 concentration.

However,PIM-1 was reported to be thermally stable at temperature up to 450°C in inert atmosphere (350°C in air), according to the initial work by Budd and McKeown[23].

In this work, using PIM-1 as a prototypical microporous polymer, we demonstrate a simple process of thermal oxidative crosslinking of independent rigid polymer chains to covalently crosslinked polymer networks with significantly enhanced molecular-sieving selectivity and exceptional gas separation performance. From a microscopic point of view, as schematically shown in Fig. 1c-f, the high-free-volume polymer matrix behaves as a series of interconnected nano-reactors, which allows sorption and fast diffusion of oxygen molecules through the gates between the interconnected cavities. Upon heating at suitable temperature window (350-450°C) in the presence of trace amounts of oxygen, we hypothesize that oxidative crosslinking of polymer chains occur at the larger bottlenecks of interconnected micropores owing to the preferential diffusion of oxygen. Such vulcanization process results in three-dimensional crosslinked networks with narrower (or closed) gates offering remarkably better size and shape selectivity while the overall free volume is still sufficiently high, allowing rapid and selective diffusion of gas molecules.

Results

Characterization of membranes. We fabricated free-standing dense PIM-1 membranes (thickness ~50 μm) by casting the solution of polymer (Fig. 2a). After thermal oxidative crosslinking at 385°C in the presence of trace amounts of oxygen (vacuum of 1 mbar) for prolonged periods (up to 24 h), the transparent membrane changed from fluorescent yellow (Fig. 2b) to dark brown as visually observed (Fig. 2c). The thermal-oxidatively crosslinked PIM-1 (termed as TOX-PIM-1 hereafter) polymer membranes became largely insoluble (gel content >95%) in solvents that readily dissolve the PIM-1 polymer, such as chloroform (Fig. 2d), tetrahydrofuran, or dichloromethane (details of solubility tests are given in Supplementary Fig. 2**)**. Furthermore, UV-vis absorption spectra and loss of photoluminescence of polymer films clearly indicate the degradation of polymer (Supplementary Fig. 3). The membranes showed weight loss of ~2 wt% owing to the thermal oxidative degradation. The skeletal density of crosslinked membranes slightly increased from 1.335±0.006 g cm^{-3} to 1.365±0.007 g cm^{-3}, while there is no substantial change in apparent bulk density (1.060-1.100 g cm^{-3}). Wide-angle X-

ray scattering confirms TOX-PIM-1 polymers remain amorphous (Supplementary Fig. 4). Thermogravimetric analysis indicated high thermal stability of both PIM-1 and TOX-PIM-1 up to ~450°C in an inert argon atmosphere (Supplementary Fig. 5). As examined by scanning electron microscopy (Supplementary Fig. 6), both PIM-1 and TOX-PIM-1 polymer membranes are defect-free and do not show observable mesoporosity, therefore the gas transport properties as measured are intrinsic values.

Mechanical properties. We found that thermal-oxidative treatment at temperature of 375-385°C along with slow thermal oxidation rate at ppm-level concentrations of oxygen for a prolonged exposure time, resulted in almost fully covalently crosslinked films that remained transparent, flexible, and mechanically resilient. A typical plot of stress-strain curve (Fig. 2e) shows that the TOX-PIM-1 polymer films after slow crosslinking become stiff but are still mechanically robust in terms of tensile strength (50-60 MPa), elongation strain at break (in the range of 4-8 %), and Young's modulus (1.2 to 1.7 Gpa) (Supplementary Fig. 7 and Supplementary Table 1). Nanoindentation confirmed the increase of hardness from 149±4.0 to 188±3.0 MPa while the Young's modulus only shows a slight increase from 1.876±0.029 to 1.885±0.039 GPa (Supplementary Fig. 8). For PIM-1 films annealed at higher concentration of oxygen (e.g. 20.9 vol.% O_2 in air), the films became brittle because of excessive oxidation. For the films annealed at higher temperature (>400°C) for prolonged periods, the samples became too brittle for stretching measurement as excessive crosslinking or degradation has occurred.

Thermal oxidative crosslinking. We confirmed the critical role of oxygen in thermal-oxidative degradation and crosslinking of the polymer membranes. PIM-1 polymer is thermally stable in inert atmosphere, with evident degradation at temperatures above 450°C in pure argon (Fig. 2f). *In situ* Fourier Transform Infrared (FTIR) spectra of gaseous products evolved during pyrolysis in thermogravimetric analyser (TGA) (Fig. 2g) indicates that the scission of ether linkages in the backbone is the dominant decomposition step since only dioxane linkages are the oxygen-containing groups, generating CO_2 as primary gaseous product (2260 cm^{-1} in the spectra), though the initiation step is not clear. In contrast, thermal-oxidative degradation of the PIM-1 polymer occurs at much lower temperature, with evident oxidation starting at 350°C in air (Fig. 2f) and CO_2 as major gaseous product

(Supplementary Fig. 9). Such oxidative degradation was confirmed by baking the polymer membranes in an oven at the same temperature in air. Alternatively, exposing the membranes in air in the temperature range of 300-450°C for prolonged periods could result in varied degree of oxidative degradation (e.g. complete degradation with CO_2 as primary product, Supplementary Fig. 9). Therefore, there is a temperature window between 350-450°C where oxidative pyrolysis could occur, as confirmed by heating PIM-1 polymer in inert purging gas at low O_2 concentrations (e.g. 200 ppm O_2) (Fig. 2f). These experiments confirm the dominant mechanism of thermal-oxidative degradation in the presence of oxygen.

We further tuned the degree of thermal-oxidative crosslinking of PIM-1 polymer using a reaction engineering approach, *via* changing the O_2 concentration, temperature, and reaction time, and tracked the evolution of gel content and molecular weight distribution. For example, the polymer heated in argon containing 200 ppm O_2 at 300-450°C underwent oxidative crosslinking and pyrolysis (Fig. 2h and Supplementary Fig. 10), rather than significant degradation in air. As the reaction temperature increase, the films changed from fluorescent yellow to dark brown and black (Fig. 2i). Characterization of these samples indicate similar physical and chemical properties as those obtained in vacuum oven for prolonged time, though they are relatively more brittle due to the high O_2 concentration (200 ppm). These TGA experiments confirmed that the optimal crosslinking temperature appears to be around 375-385°C (tunable depending on the O_2 concentration), and a weight loss of 1.5-2.5 wt% due to thermal oxidation would be sufficient to induce crosslinking. Therefore, we are able to tune the extent of oxidation and crosslinking based on Arrhenius-like chemical reaction kinetics (Supplementary Note 1 and Supplementary Fig. 11), and terminate the reaction at the suitable point under controlled conditions, to avoid excessive degradation or carbonization.

The thermal-oxidatively crosslinked polymer films were dissolved in chloroform, as shown in Fig. 2d, with non-dissolved gel and soluble solution separated. The molecular weight distribution in the soluble polymer solution, evolves from a peak molecular weight of 100 kDalton to a disperse mixture of fragments of molecular weight up to several hundred (Fig. 2j), indicating that random oxidative chain scission occurred involving the backbone. At the same time, the weight fraction of insoluble gel

content increased (Fig. 2k); therefore we propose that oxidative chain scission and *in situ* covalent crosslinking occurred. Similar changes were observed for the polymer films exposed to varied temperatures (Supplementary Fig. 12). Furthermore, *ex situ* FTIR spectra (Supplementary Fig. 13) of TOX-PIM-1 polymer films confirmed that the membranes remain in the polymeric state rather than being carbonized, but the presence of weak peaks corresponding to residual carbonyl and weak hydroxyl groups provides a clear evidence of oxidation. The nitrile (C≡N) groups are relatively stable and peaks associated with C=N groups were not observable, an evidence denying the mechanism of trimerization. To summarize, these characterization analyses suggest a thermal-oxidative degradation mechanism following reaction pathways of free-radicals induced oxidative chain scission, and *in situ* covalent crosslinking. In addition to covalent crosslinking bonds, the local oxidation of polymer may also introduce intermolecular or intramolecular interactions *via* hydrogen bonding between ether linkages of the backbone and residual oxidized groups (e.g. carboxylic acid) in polymer chains (Supplementary Fig. 14), as experimentally observed in carboxylated PIMs[37]. The hydrogen bonding could form physical crosslinking and tighten the chains locally in the polymer matrix, along with the covalent crosslinking bonds.

Gas sorption properties. The gas solubility in polymer membranes were probed with a series of gas sorption measurements. Low temperature gas sorption/desorption is a widely used method to probe the pore structure of microporous materials, however, it is not very effective for microporous polymers. In particular, the N_2 adsorption of TOX-PIM-1 membranes at 77 K show an unexpected gate-opening effect, as shown in Fig. 3a, which is related to the kinetically-limited diffusion of N_2 molecules through the dynamically open-and-shut gates connecting free volume elements, as illustrated in Fig. 1e. Such a gate-opening phenomenon indicates the complicated molecular interactions at low temperature (77 K), and though it has been reported in other works, which is not well understood for PIM-1 and other high free volume polymers[38-39]. Gas sorption properties of CO_2, CH_4 and N_2 were also measured at 273 K (Fig. 3b). The TOX-PIM-1 polymer membrane showed slightly lower CO_2 sorption than that of PIM-1. Pore size distributions derived from CO_2 sorption isotherms at 273 K based on non-local density functional theory (NLDFT) methods (Supplementary Fig. 15) show an apparent loss of ultra-

microporosity (size smaller than 7 Å), in agreement with our proposed mechanism of narrower bottlenecks of the interconnected micropores. At higher room temperature (295 K), gas sorption isotherms (Fig. 3c) follow the dual mode sorption mechanism without observable plasticization at high pressure. The solubility of various gases (295 K, 1 bar) in TOX-PIM-1 and was not significantly altered from the unmodified PIM-1.

Gas transport properties. Single-gas permeations through polymer membranes were performed at 295 K with industrially-important gas molecules with different kinetic diameters, including H_2 (2.89 Å), CO_2 (3.3 Å), O_2 (3.46 Å), N_2 (3.64 Å), and CH_4 (3.8 Å), as shown in Fig. 3d. Gas transport in microporous PIM-1 polymer can still be illustrated with the solution-diffusion model, where the permeability coefficient (P) is a product of solubility (S) and diffusion coefficient (D), $P = S \times D$. The gas permeability of unmodified PIM-1 follows the sequence of CO_2>H_2>O_2>CH_4>N_2, owing to the combined effects of sorption (e.g condensable CO_2 and CH_4) and diffusion (gas molecules with different sizes). After thermal-oxidative crosslinking at 385°C under vacuum of 1 mbar, the TOX-PIM-1 membrane showed significantly lower gas permeability for larger molecules (N_2 and CH_4) by two magnitudes, while smaller gas molecules (H_2, CO_2, O_2) maintained considerably high permeability, giving a more remarkable molecular sieving function. Figure 3g shows a representative plot of selectivity *versus* permeability for an industrially important CO_2/CH_4 gas pair along with the upper bound limit of polymer membranes. For a representative TOX-PIM-1 membrane crosslinked at 385°C, the CO_2/CH_4 selectivity increased up to 70 with a high CO_2 permeability of 1100 Barrer [1 Barrer = 1×10^{-10} cm^3 cm cm^{-2} s^{-1} $cmHg^{-1}$ at standard temperature and pressure (STP)]. The significantly enhanced gas selectivity along with high permeability push the overall gas transport properties to surpass the upper bound that has been limiting the polymer membranes for decades. To the best of our knowledge, the overall separation performance of TOX-PIM-1 membranes is higher than all existing soluble polymers including commercial polymers[40], soluble PIMs[41], and compares very well against TR polymers[18,31,34,42-44].

The gas solubilities at 295 K and 1 bar are derived from the sorption isotherms (Fig. 3c) and correlate well with the critical temperature of gas molecules (Fig. 3e). Based on the solubility and gas

permeability (Fig. 3d), gas diffusion coefficients (at 1 bar, 295 K) are derived as shown in Fig. 3f (detailed data are given in Supplementary Table 2), proving an evident shape-selective molecular sieving effect. The increase in diffusivity selectivity (D_A/D_B) and constant solubility selectivity (S_A/S_B) confirm that the significant improvement of gas selectivity is attributed to the structural modification of the gateways between the free volume cavities.

The separation of gas mixtures were also examined for the TOX-PIM-1 membranes, including CO_2/CH_4 and CO_2/N_2 (Supplementary Fig. 16). Figure 3 h and i show the selectivity of CO_2/CH_4 and CO_2/N_2 *versus* CO_2 fugacity for separation of corresponding gas mixtures. In a mixed gas atmosphere, gas molecules compete for sorption sites, particularly at high pressure. Therefore, we observed a decrease in the CO_2/CH_4 selectivity at high pressure, which nevertheless is still as high as 30 over CO_2 fugacity of 5-10 bar, a range of interest for industrial natural gas purification. In the case of CO_2/N_2 separation, the selectivity is above 40 at low pressure of 2 bar while the CO_2 permeability is maintained above 1000 Barrer. Such performance is of potential for efficient separation of CO_2 from flue gas emitted from coal-fired power plants at atmospheric pressure.

Tunable gas transport properties. We tuned the gas transport properties by controlling the degree of polymer crosslinking *via* controlling temperature (Fig. 4a-b), reaction time (Fig. 4c-d), and O_2 concentration (Fig. 4e-f). At excessive oxidative pyrolysis conditions (e.g. weight loss about 3 wt% at 400°C under vacuum), the CO_2 permeability shows a significant drop (<100 Barrer) and the gas transport properties became close to those of carbon molecular sieve membranes. In an extreme instance, by baking the polymer at 385°C in air for 10 min (weight loss about 2.5 wt%), the CO_2/CH_4 selectivity was also enhanced up to 70, while the CO_2 permeability maintained as high as ~500 Barrer, though the membrane became brittle due to excessive decay of mechanical properties. We summarize the gas transport properties obtained at various thermal oxidation conditions (Supplementary Table 3). A typical Robeson plot of CO_2/CH_4 selectivity versus CO_2 permeability in Fig. 4g shows the overall trends of significant enhancement of selectivity while the gas permeability decrease although maintaining at a significant level over commercial polymer membranes.

The tunable gas transport properties of other industrially important gas pairs, such as O_2/N_2, CO_2/N_2, H_2/N_2, and H_2/CH_4, follow similar trends as shown in Fig. 5. For example, the O_2/N_2 selectivity could be enhanced to as high as ~8.0 while the permeability remains as high as 250 Barrer. Such remarkable O_2/N_2 separation performance is very promising for applications in N_2 separation or oxygen enrichment (for oxyfuel combustion). The notable H_2 separation over N_2 and CH_4 are attractive for practical applications in H_2 recovery and natural gas purification. Interestingly, the gas transport data of TOX-PIM-1 membranes obtained from various experimental conditions seem to follow a continuous trend in the upper bound plot, in agreement with the tunable gas diffusivity and structural transformation of micropore structure.

Aging behaviour. A particular concern for the use of glassy polymeric materials as gas separation membranes is their performance over several years, where the glassy polymer is expected to age. Thermodynamically, the rigid polymer chains still tend to pack space efficiently due to the relative freedom of conformation and rotation, and intermolecular noncovalent interactions (chain entanglements, hydrogen bonding, etc) as the system tends to reach equilibrium. The gas permeability of PIM-1 shows gradual loss but at rates lower than other high free volume polymers, such as poly(1-trimethylsilyl-1-propyne) (PTMSP)[45], whilst the selectivity slightly increases under continuous vacuum. The aging of thermal-oxidatively crosslinked PIM-1 membranes followed a decrease in gas permeability and increase in selectivity under vacuum over initial 3-5 days, but then slowly stabilized over prolonged time of about one year (Supplementary Fig. 17). Some representative data are shown for a representative CO_2/CH_4 gas pair in Fig. 4h-i, confirming that the gas transport properties of aged crosslinked polymer network remained at a significant level. In a broader context, the crosslinked network may not suffer from chain conformational relaxation in other molecular-level separations involving solvent swelling, such as pervaporation and organic solvent nanofiltration (OSN)[46].

Discussion

Thermal treatment of organic materials at high temperature involves complex chemical reactions (e.g. pyrolysis, combustion, degradation, crosslinking, carbonization, etc), heat and mass transfer, and changes of physicochemical properties. Controlled thermal processing is widely used, such as

pyrolysis, gasification and combustion of fuels, gasification and oxidation of biomass (or polymers and coal) with the existence of steam or O_2 for producing carbon molecular sieves (CMS) and activated carbon (dominant adsorbents). In the membrane field, Koros and co-workers found the critical role of oxygen in controlling the atmosphere of pyrolysis to tailor the gas separation performance of CMS membranes (known as O_2 doping)[47-48]. However, the CMS membranes are normally heated at temperatures above 500°C, consequently losing mechanical strength. Instead, thermochemical transformation at relatively lower temperature is desired to retain the mechanical strength. For example, a unique class of thermally rearranged (TR) polymers were derived from polyimides containing ortho-positioned functional groups (e.g. -OH and -SH) by heating at 350-450°C[18]. The TR polymers start from non-porous glassy polyimides, through thermochemical reactions, to insoluble and infusible molecular sieving materials with hour-glass shaped micropore structure, while the gas transport properties change from the region of high-selectivity/low-permeability to significantly higher permeability and slight loss in selectivity (Fig. 4g).

In contrast, our novel approach starts from microporous PIM-1 polymer precursor and transformation to crosslinked polymer networks *via* thermal oxidative crosslinking reactions at intermediate temperatures, which are different from those reactions occurred in CMS (e.g. controlled oxidation and carbonization at high temperature) or TR polymers (rearrangement). Our TOX-PIM-1 membranes showed remarkably enhanced selectivity while the gas permeability decreased but remained at a significant level that is two-to-three magnitude higher than commercial polymers, for a number of gas-pairs and comparable to that of CMS or TR membranes (see a summary of data in Supplementary Table 4). Sorption data shows little change in the overall solubility of gases, before and after thermal processing, indicating that mild chemical changes have taken place primarily at these gateways with minimal impact on the overall free volume. This is corroborated by the similar rates of aging, or chain conformation observed within the PIM-1 and the major portions of network TOX-PIM-1, albeit from different starting points on the Robeson plot (Fig. 4i). Therefore, the loss in permeability in the PIM-1 material and its enhanced selectivity arises from thermo-oxidative closure of the bottlenecks between high-free-volume domains.

The novelty of our work on the controlled thermal oxidative crosslinking of the PIM-1 polymer, is also different from the paper reported by Li *et al* on thermally treated PIM-1 polymer[36]. The paper of Li *et al* describes a poorly-controlled thermal processing of PIM-1 at temperature of 300°C, and reported that both permeability and selectivity are enhanced (see Fig. 4g) whilst inducing crosslinking without the generation of volatile side-products[36]. In contrast, we find that membranes annealed at 300°C under vacuum or inert atmosphere remain stable, with our strong evidence from molecular weight distribution, IR spectra, TGA data, and gas permeation data. In fact, the earliest work by Budd and McKeown already found that PIM-1 is stable at temperature up to 450°C in inert atmosphere (350°C in air), even when heated at 300°C for 24 h[23]. It is also notable that Du *et al*. were unable to reproduce the claims by Li *et al*. whilst using a higher temperature (375ºC) and shorter times (45 minutes)[49]. Du *et al* indicated that the annealing time was not sufficiently long enough for crosslinking (likely owing to lower O_2 concentration in high-purity inert purge gas), as proven by our kinetic-study at 385ºC in Fig. 4c. According to the Arrhenius-like expression of oxidative degradation kinetics with temperature (Supplementary Fig. 11), it is highly unlikely that crosslinking reactions can occur at 300ºC within the two days that Li *et al*. have annealed their materials. Our extensive experimental data provide solid evidence supporting a different and more reasonable thermal oxidative degradation mechanism. Furthermore, our understandings of the phenomenon of thermal oxidative crosslinking of PIM-1 polymer allow us to precisely tune the reaction kinetics and the structure of micropores in the membrane, and consequently tailor the gas diffusivity and separation performance.

The reaction mechanism merits more discussion. Recently, a decarboxylation-induced crosslinking mechanism has been proposed by Koros and co-workers for carboxylic acid-containing polyimides (at 389°C in inert atmosphere) [50], and carboxylated PIMs by Du and Guiver (at 375°C in inert atmosphere)[37,49]. Both studies have proposed free-radical induced covalent crosslinking following the decarboxylation reactions. In this study, during thermal treatment at similar temperature range (over 350-400°C, preferably 375-385°C) in the presence of oxygen, oxidation and crosslinking occurred. It is generally acknowledged that thermal oxidation (and oxidation induced by light or ozone) of polymer involves free-radical chain reactions, including initiation (e.g. hydrogen abstraction or weak links along

the chain), propagation, and termination (e.g. crosslinking)[51]. According to the well-known chain reaction mechanism[51], the oxygen reacts with the free radical (R·) forming peroxy radical (ROO·) which can further abstract a hydrogen from adjacent polymer chain to generate hydroperoxide (ROOH). The instable hydroperoxide can split into two free radicals (RO· and ·OH), which would continue to propagate to initiate a new free-radical chain reactions until termination occurs, such as crosslinking due to the combination of radical sites on adjacent chains. In the temperature window of 350-450°C (or preferably, 350-400°C), the possible reaction sites could involve the methyl groups, dioxane linkages, and spiro-carbon centre, while the fused aromatic rings should be relatively more stable. The weaker methyl groups on the spiro-carbon centre are possible initial sites for abstraction of hydrogen. Mass balances obtained in TGA (**Fig. 2h**) confirmed that very little amount of weight loss (1.5-2.5 wt%) is sufficient to achieve high degree of crosslinking with excellent molecular sieving properties. The chemical formula for one repeating unit of PIM-1 is $C_{29}H_{20}N_2O_4$, corresponding a molecular weight of 460.5 g mol^{-1}. A little amount of weight loss up to 1.5-2.5 wt% corresponds to 7-11.5 g for 1 mol repeating unit, idealy, abstraction of several hydrogen atoms from the four methyl groups (-CH_3, containing 12 H atoms), or abstraction of methyl radicals (·CH_3) would be sufficient. Of course, the evolution of molecular weight distribution indicates a mechanism of random scission involving the backbone, rather than simply abstraction of side groups. Therefore, mechanisms of both oxidative chain scission and covalent crosslinking merit further study in the future.

In practice, polymer separation membranes can be fabricated using established techniques and module designs (flat sheet, spiral wound, or hollow fibers) followed by post-treatment. Indeed, many parameters are involved in the thermal oxidative crosslinking, including the temperature, oxygen concentration in the polymer and purge gas, heating rate, and reaction time. But we demonstrate that these parameters could be carefully controlled in our experiments or more delicately controlled TGA-like reactor, using a chemical reaction engineering approach. We confirmed that the crosslinking through the thick PIM-1 polymer films could be achieved. We have also demonstrated that the oxidative crosslinking is effective for PIM-1 polymer thin films coated on silicon or glass substrates,

which are dense and defect-free as examined by scanning electron microscopy (SEM) (Supplementary Fig. 18). Similarly, we expect that thin films coated on thermally stable porous ceramic membrane supports can be exposed to heat treatment at controlled atmosphere, potentially allowing the scale up of our process.

Because it is not possible to achieve a completely oxygen-free atmosphere in practice, trace amounts of oxygen absorbed in organic microporous materials can always induce oxidation upon thermal processing and consequently resulting in significantly different properties. Our approach on PIM-1 polymer represents a rational design and transformation of PIMs polymers, which is of broader fundamental significance to post-synthetic modification of the structure of channels and pores in a wide range of porous materials, such as MOFs[52], porous organic molecules[53-56], covalent organic frameworks (COFs)[57], and graphene-based carbon materials[58-60].

In summary, we report the phenomenon of thermo-oxidative degradation and crosslinking of PIM-1 polymer with a broad distribution of microporosity, and demonstrate rational control of this process to tune the micropore structure of membranes and molecular sieving functions. Our approach leads to highly permeable and selective membranes that show great potential for molecular-level separations in energy and environmental processes, such as capturing CO_2 from flue gas, air separation, biogas and natural gas production, H_2 production, separation of hydrocarbons (olefin/paraffin) in petrochemical industries, pervaporation, and organic solvent nanofiltration. In a broad context, our method is not limited to membrane applications, the controlled thermally crosslinked polymer frameworks can be used as molecular sieves for other applications, for example, solid sorbents for sorption of gas and chemicals. Furthermore, this broader principle is instructive in utilizing other porous polymeric materials and tuning the topology and structure of channels and pores for a wide range of applications.

Methods

Synthesis of polymer. The PIM-1 polymer was synthesised following the method invented by Budd and McKeown[23], from polycondensation reaction of 3,3,3□ ,3□-tetramethyl-1,1□- spirobisindane-5,5□ ,6,6□-tetrol (TTSBI, 30 mmol, Alfa Aesar) and 2,3,5,6-tetrafluoroterephthalonitrile (TFTPN, 30 mmol, Matrix Scientific) in the presence of K_2CO_3 (60 mmol, Aldrich) in anhydrous dimethylformamide (200 mL). After the mixture has been stirred at 60°C for about 48 h, the polymer was purified by dissolving in chloroform and re-precipitation

from methanol, filtered and dried in vacuum oven at 110°C for overnight. The molecular weight of purified polymer was determined from gel permeation chromatography (GPC), giving an average molecular weight of M_n= 80, 000 to 100,000 dalton and a polydispersity (PDI) of 2.0.

Preparation of membranes. Thick dense membranes were prepared by casting polymer solution in chloroform. Nondissolved particles were removed by filtration through PTFE filters or by centrifugation. Polymer solutions were casted on clean glass substrate in a glove box. After the solvent has been slowly evaporated at room temperature in two days, the dry free-standing membranes were obtained and exposed to methanol soaking for overnight and dried in air. After, the membrane was dried in a vacuum oven at 120°C for 24 h. Thin films were prepared by spin coating of diluted PIM-1 solution in chloroform on different substrates.

Thermal analyses. Thermal analyses of polymer films were performed in a thermogravimetric analyser (TGA) to study the thermal degradation and thermal oxidative degradation in well-controlled atmosphere. The gas species evolved from the TGA was analyzed by a FTIR. The gas atmosphere includes Argon (Air products), Air (zero grade, air products), and O_2/Argon mixture (200 ppm O_2, balance argon, BOC). In one series of experiments, polymer films were dynamically heated from room temperature to 1000°C at 10°C min^{-1} in inert atmosphere or in air. Another series of experiments were carried out using O_2/Argon mixture (200 ppm O_2, balance argon, BOC). A batch of dense polymer films (~5 mg, dimension of 3×3 mm) were heated at 120°C for 1 h under continuous flow of purging gas to remove moisture and residual gases, then heated at 10°C min^{-1} to varied temperature (300-450°C), then kept at the set-point temperature for 2 h.

Thermal oxidative crosslinking. The PIM-1 membranes were exposed to thermal treatment under controlled atmosphere in a high-temperature vacuum oven (Heraeus, 20-400°C). The vacuum oven was modified allowing operation in controlled vacuum or purging mode. The pressure was monitored continuously by pressure transmitters (Keller Ltd, UK). A series of experiments were performed by heating the polymer at different temperature under continuous controlled vacuum (1 mbar). Flat polymer films were placed on the plate in the vacuum oven and heated under vacuum at 120°C for 3 h, then heated to final temperature at 10°C min^{-1}. Then the samples were maintained at the temperature for extended time up to 24 h. Another series of experiments were carried out by heating PIM-1 membranes in the vacuum oven at 385°C, with the vacuum pressure controlled at 1, 10, 20, 50, 100, 200 mbar.

Alternatively, we controlled the atmosphere of heat treatment by purging inert gases containing low concentration of O_2 (0-200 ppm), including high purity argon (B.I.P. grade, O_2 <10 ppb, Air products), and O_2 balanced with argon (BOC, UK), with nominal O_2 concentration at 10(9.2), 50(55), 100(104), 200(215) ppm, where the value in parentheses are the calibrated concentration. The flow rate (2 L min^{-1}) was controlled by a metering valve. The polymer films were placed on the heating plate in the oven, and exposed to vacuum at 120°C under vacuum for 1 h, then purging gas was introduced to the oven to pressurize the oven close to 1000 mbar, then vacuum was switched on again to reduce the pressure. After at least five cycles of vacuum-pressurization, the samples were exposed to continuous flow of purging gas for a certain period.

In extreme cases, the polymer films were simply baked in air. In one series of experiment, the polymer films were heated in air from 120°C to 385°C at 10°C min^{-1}. Rapid change of colour from fluorescent yellow to brownish was observed when the temperature was above 350°C. During this heating stage, the polymer films were turned over frequently, manually with tweezers. When the temperature reached to 385°C, the brown-colour thermally oxidized polymer films were removed from the oven to avoid excessive degree of degradation (too brittle for gas permeation tests) due to the fast reaction rate as shown in TGA (as evidenced by further colour changing to black), and cooled down naturally to ambient temperature. Alternatively, the oven was switched to vacuum mode. In the mean time, the power of the oven was turned off allowing the films to cool down to room temperature under vacuum. In another series of isothermal experiment, fresh membranes were moved from ambient condition to the preheated oven (385°C) and baked for 10 min, and removed from the oven immediately. The three methods gave similar degree of degradation of polymer, with weight loss at ~2.5 wt%. The volatile products released should be connected to ventilation.

Characterization. Scanning electron microscopy (SEM) analysis of membranes was performed using a Hitachi S5500 microscope. The polymer films were fractured in liquid nitrogen and coated with a thin layer of gold. The molecular weight of polymer was quantified by gel permeation chromatography (GPC) calibrated with polystyrene standards. UV–visible absorption spectra of polymer thin film (~100 nm,) were measured using a Hewlett Packard 8453 UV-Vis spectrometer. Steady-state photoluminescence excitation measurements were

measured with a CARY Eclipse fluorescence spectrophotometer, at an excitation wavelength of 420 nm. The FTIR spectra were measured using an Infrared spectrometer in transmission mode, or using an attenuated total reflectance (ATR) cell. The skeletal density of polymer films (100-200 mg) was measured using a Micromeritics Accupyc 1340 helium pycnometer. Before density measurements, all samples were evacuated thoroughly under vacuum at 150 °C for 5 hours. The apparent bulk density was measured from the gravimetric method, using films with uniform thickness, and quantifying the mass and size. The gel fractions of crosslinked polymer films were quantified by soaking them in solvent and the weight fraction of undissolved gel was quantified, while the dissolved fraction of polymer was examined with GPC to quantify the evolution of molecular weight distribution. Wide angle X-ray scattering was performed with a Bruker D8 machine operated at 40 mA and 40 kV using Cu Kα radiation with a step of 0.02° per second.

Mechanical properties. Tensile tests of polymer films were carried out at a home-made stretcher machine. Polymer films with thickness in the range of 50-80 um were cut into thin slices with an effective length of ~20 mm and a width of ~2 mm, with the accurate value determined from high-resolution photos and calibrations from known length. The films were stretched for 0.02 mm in each step with a relaxation time of 30 s, giving an apparent strain rate of ~4×10^{-5} s^{-1}. The average value of Young's modulus was derived from the initial slope. The tensile strength at break and elongation at break were also measured. Nanoindentation of surfaces of polymer membranes were performed at ambient temperature using a sharp Berkovich tip in the continuous stiffness measurement (CSM) mode on an MTS NanoIndenter® XP (MTS Corp., Eden Prairie, MN). The indenter axes were aligned normal to the membrane planes. The average values of the Young's modulus (E) and the hardness (H) were extracted from the force-displacement P-h curves over depths of 100–1000 nm, with a series of 20 measurements at different locations.

Gas sorption. Low-pressure gas sorption was performed using a Micromeritics ASAP 2020 instrument with pressure up to 1 bar. Dense polymer membranes (~0.1 g) with thickness of ~50 µm were cut into small pieces, loaded into the apparatus and degassed at 120 °C under high vacuum(<10^{-6} bar). After the mass being measured, the samples were further degassed under high vacuum prior to the gas sorption measurement. Nitrogen adsorption-desorption isotherms were measured at 77 K and 273 K, respectively. The sorption isotherms of CO_2 and CH_4 were also measured at 273 K. The specific surface area was calculated based on the Brunauer-Emmett-Teller (BET) model and the pore size distribution was derived from non-local density functional theory (NLDFT) model from N_2 isotherms at 77 K, or from CO_2 sorption isotherms at 273 K when the sorption of N_2 was subjected to kinetic control. High-pressure pure-gas sorption isotherms were measured using a home-made dual-volume pressure-decay apparatus at pressure up to 35 bar and room temperature of 295 K. A batch of polymer films was heated at 120°C under high vacuum for 12 h. After measurement of the mass, the films were loaded in the sample cell and further evacuated for 12 h prior to sorption measurements. The amount of gas sorption was calculated from the mass balance of gas molecules based on the equation of gas states, using the equilibrium pressure calibrated with compressibility factors. The measurements followed the sequence of H_2, O_2, N_2, CH_4, and CO_2. The samples were thoroughly evacuated between measurements of each gas.

Gas permeation. Pure gas permeation tests were carried out at temperature of 22°C and feed pressure of 4 bar, using a constant-volume pressure-increase apparatus. The mixed gas permeation properties were measured in another membrane cell using the constant-pressure variable-volume method. The membrane was exposed to certified gas mixtures (BOC, UK) of CO_2/CH_4 (50/50 vol.%) and CO_2/N_2 (50/50 vol.%) with feed pressure up to 35 bar at room temperature (22°C), with a stage cut (ratio of flow rates of permeate to feed) less than 1 %. The gas compositions were analyzed by a gas chromatograph (GC-2014, Shimadzu). Details are given in the Supplementary Methods.

Molecular simulation. Molecular dynamics (MD) simulations were performed with the Materials Studio software package (Accelrys Inc, CA, USA). In one amorphous cell, four PIM-1 polymer chains with 10 repeating units were constructed at 298 K. For the thermally oxidized and crosslinked polymers, the reaction mechanisms are very complicated. Here, we use the MD simulation primarily to understand the intermolecular interactions (e.g. hydrogen bonding), and packing of short polymer segments. To mimic the oxidative chain scission, 20 short chains containing two repeating units of PIM-1 with oxidised groups (e.g. carboxylic acid groups, -COOH) were constructed in another amorphous cell at 298 K as well. For those covalently crosslinked polymers, due to the difficulty to analyse the chemical structure, they were not simulated. The Berendsen algorithm with a decay constant of 0.1 ps was used to control the temperature and pressure of each cell. The specific procedures are as follows: (1) energy minimization; (2) 50 ps NVT-MD simulation at 600 K; (3) 50 ps NPT-MD simulation at 600 K at 1 bar; (4) 50 ps NPT-MD simulation at 298 K at 1 bar; (5) 50 ps NPT-MD

simulation at 298 K at 10 bar with a step of 1.0 fs; (6) 50 ps NVT-MD at 298 K; (7) 50 ps NPT at 298 K at 1 bar. The Ewald summation method was used to calculate the non-bond interactions with an accuracy of 0.001 kcal/mol. Hydrogen bonding was automatically monitored by the software based on a list of hydrogen-bonding scheme (N, O, S, and Halogens).

References

1. Gin, D. L. & Noble, R. D., Designing the Next Generation of Chemical Separation Membranes. *Science* **332**, 674-676 (2011).

2. Yampolskii, Y. & Freeman, B. D., *Membrane gas separation*. (John Wiley & Sons, Ltd, 2010).

3. Paul, D. R., Creating New Types of Carbon-Based Membranes. *Science* **335**, 413-414 (2012).

4. Cheetham, A. K., Férey, G., & Loiseau, T., Open-Framework Inorganic Materials. *Angew. Chem., Int. Ed.* **38**, 3268-3292 (1999).

5. Corma, A. *et al.*, Supramolecular self-assembled molecules as organic directing agent for synthesis of zeolites. *Nature* **431**, 287-290 (2004).

6. Lai, Z. *et al.*, Microstructural Optimization of a Zeolite Membrane for Organic Vapor Separation. *Science* **300**, 456-460 (2003).

7. Varoon, K. *et al.*, Dispersible Exfoliated Zeolite Nanosheets and Their Application as a Selective Membrane. *Science* **334**, 72-75 (2011).

8. Yaghi, O. M. *et al.*, Reticular synthesis and the design of new materials. *Nature* **423**, 705-714 (2003).

9. Furukawa, H. *et al.*, Ultrahigh Porosity in Metal-Organic Frameworks. *Science* **329**, 424-428 (2010).

10. Park, K. S. *et al.*, Exceptional chemical and thermal stability of zeolitic imidazolate frameworks. *Proc. Natl. Acad. Sci. U. S. A.* **103**, 10186-10191 (2006).

11. Hayashi, H. *et al.*, Zeolite A imidazolate frameworks. *Nat. Mater.* **6**, 501-506 (2007).

12. Corma, A. *et al.*, A large-cavity zeolite with wide pore windows and potential as an oil refining catalyst. *Nature* **418**, 514-517 (2002).

13. Banerjee, R. *et al.*, High-throughput synthesis of zeolitic imidazolate frameworks and application to CO2 capture. *Science* **319**, 939-943 (2008).

14. Caro, J., Are MOF membranes better in gas separation than those made of zeolites? *Current Opinion in Chemical Engineering* **1**, 77-83 (2011).

15. Freeman, B. D., Basis of Permeability/Selectivity Tradeoff Relations in Polymeric Gas Separation Membranes. *Macromolecules* **32**, 375-380 (1999).

16. Robeson, L. M., Correlation of separation factor versus permeability for polymeric membranes. *J. Membr. Sci.* **62**, 165-185 (1991).

17. Robeson, L. M., The upper bound revisited. *J. Membr. Sci.* **320**, 390-400 (2008).

18. Park, H. B. *et al.*, Polymers with Cavities Tuned for Fast Selective Transport of Small Molecules and Ions. *Science* **318**, 254-258 (2007).

19. Holst, J. R., Trewin, A., & Cooper, A. I., Porous organic molecules. *Nat Chem* **2**, 915-920 (2010).

20. Du, N. *et al.*, Polymer nanosieve membranes for CO2-capture applications. *Nat. Mater.* **10**, 372-375 (2011).

21. Carta, M. *et al.*, An Efficient Polymer Molecular Sieve for Membrane Gas Separations. *Science* **339**, 303-307 (2013).

22. Budd, P. M. *et al.*, Polymers of intrinsic microporosity (PIMs): Robust, solution-processable, organic nanoporous materials. *Chem. Commun.* **10**, 230-231 (2004).

23. Budd, P. M. *et al.*, Solution-Processed, Organophilic Membrane Derived from a Polymer of Intrinsic Microporosity. *Adv. Mater.* **16**, 456-459 (2004).

24. McKeown, N. B. *et al.*, Polymers of intrinsic microporosity (PIMs): Bridging the void between microporous and polymeric materials. *Chemistry - A European Journal* **11**, 2610-2620 (2005).

25. Budd, P. M. *et al.*, Gas separation membranes from polymers of intrinsic microporosity. *J. Membr. Sci.* **251**, 263-269 (2005).

26. McKeown, N. B. & Budd, P. M., Polymers of intrinsic microporosity (PIMs): Organic materials for membrane separations, heterogeneous catalysis and hydrogen storage. *Chem. Soc. Rev.* **35**, 675-683 (2006).

27. Ghanem, B. S. *et al.*, High-performance membranes from polyimides with intrinsic microporosity. *Adv. Mater.* **20**, 2766-2771 (2008).

28. Preston, G. M., Carroll, T. P., Guggino, W. B., & Agre, P., Appearance of Water Channels in Xenopus Oocytes Expressing Red Cell CHIP28 Protein. *Science* **256**, 385-387 (1992).

29. Doyle, D. A. *et al.*, The Structure of the Potassium Channel: Molecular Basis of K+ Conduction and Selectivity. *Science* **280**, 69-77 (1998).

30. Heuchel, M. *et al.*, Atomistic packing model and free volume distribution of a polymer with intrinsic microporosity (PIM-1). *J. Membr. Sci.* **318**, 84-99 (2008).

31. Park, H. B. *et al.*, Thermally rearranged (TR) polymer membranes for CO2 separation. *J. Membr. Sci.* **359**, 11-24 (2010).

32. Bezzu, C. G. *et al.*, A Spirobifluorene-Based Polymer of Intrinsic Microporosity with Improved Performance for Gas Separation. *Adv. Mater.* **24**, 5930-5933 (2012).

33. Ghanem, B. S., Swaidan, R., Litwiller, E., & Pinnau, I., Ultra-Microporous Triptycene-based Polyimide Membranes for High-Performance Gas Separation. *Adv. Mater.* **26**, 3688-3692 (2014).

34. Carta, M. *et al.*, Triptycene Induced Enhancement of Membrane Gas Selectivity for Microporous Tröger's Base Polymers. *Adv. Mater.* **26**, 3526-3531 (2014).

35. Song, Q. *et al.*, Photo-oxidative enhancement of polymeric molecular sieve membranes. *Nat. Commun.* **4**, 1918 (2013).

36. Li, F. Y., Xiao, Y., Chung, T.-S., & Kawi, S., High-Performance Thermally Self-Cross-Linked Polymer of Intrinsic Microporosity (PIM-1) Membranes for Energy Development. *Macromolecules* **45**, 1427-1437 (2012).

37. Du, N. *et al.*, High-performance carboxylated polymers of intrinsic microporosity (PIMs) with tunable gas transport properties. *Macromolecules* **42**, 6038-6043 (2009).

38. Weber, J., Du, N., & Guiver, M. D., Influence of intermolecular interactions on the observable porosity in intrinsically microporous polymers. *Macromolecules* **44**, 1763-1767 (2011).

39. Weber, J., Su, Q., Antonietti, M., & Thomas, A., Exploring polymers of intrinsic microporosity - Microporous, soluble polyamide and polyimide. *Macromol. Rapid Commun.* **28**, 1871-1876 (2007).

40. Abetz, V. *et al.*, Developments in membrane research: from material via process design to industrial application. *Advanced Engineering Materials* **8**, 328-358 (2006).

41. Du, N., Park, H. B., Dal-Cin, M. M., & Guiver, M. D., Advances in high permeability polymeric membrane materials for CO2 separations. *Energy Environ. Sci.* **5**, 7306-7322 (2012).

42. Han, S. H. *et al.*, Highly gas permeable and microporous polybenzimidazole membrane by thermal rearrangement. *J. Membr. Sci.* **357**, 143-151 (2010).

43. Choi, J. I. *et al.*, Thermally rearranged (TR) poly(benzoxazole-co-pyrrolone) membranes tuned for high gas permeability and selectivity. *J. Membr. Sci.* **349**, 358-368 (2010).

44. Han, S. H. *et al.*, Thermally Rearranged (TR) Polybenzoxazole: Effects of Diverse Imidization Routes on Physical Properties and Gas Transport Behaviors. *Macromolecules* **43**, 7657-7667 (2010).

45. Nagai, K. *et al.*, Poly[1-(trimethylsilyl)-1-propyne] and related polymers: Synthesis, properties and functions. *Prog. Polym. Sci.* **26**, 721-798 (2001).

46. Gorgojo, P. *et al.*, Ultrathin Polymer Films with Intrinsic Microporosity: Anomalous Solvent Permeation and High Flux Membranes. *Adv. Funct. Mater.*, DOI: 10.1002/adfm.201400400 (2014).

47. Kiyono, M., Williams, P. J., & Koros, W. J., Effect of pyrolysis atmosphere on separation performance of carbon molecular sieve membranes. *J. Membr. Sci.* **359**, 2-10 (2010).

48. Kiyono, M., Williams, P. J., & Koros, W. J., Generalization of effect of oxygen exposure on formation and performance of carbon molecular sieve membranes. *Carbon* **48**, 4442-4449 (2010).

49. Du, N., Dal-Cin, M. M., Robertson, G. P., & Guiver, M. D., Decarboxylation-Induced Cross-Linking of Polymers of Intrinsic Microporosity (PIMs) for Membrane Gas Separation. *Macromolecules* **45**, 5134-5139 (2012).

50. Kratochvil, A. M. & Koros, W. J., Decarboxylation-Induced Cross-Linking of a Polyimide for Enhanced CO2 Plasticization Resistance. *Macromolecules* **41**, 7920-7927 (2008).

51. Welsh, W. J., *Thermal-oxidative stability and degradation of polymers, in Physical Properties of Polymers Handbook (Editor, James E. Mark)*. (American Institute of Physics, Woodbury, New York, 1996).

52. Bae, T.-H. *et al.*, A High-Performance Gas-Separation Membrane Containing Submicrometer-Sized Metal–Organic Framework Crystals. *Angew. Chem., Int. Ed.* **49**, 9863-9866 (2010).

53. Tozawa, T. *et al.*, Porous organic cages. *Nat. Mater.* **8**, 973-978 (2009).

54. Jones, J. T. A. *et al.*, Modular and predictable assembly of porous organic molecular crystals. *Nature* **474**, 367-371 (2011).

55. Bushell, A. F. *et al.*, Nanoporous Organic Polymer/Cage Composite Membranes. *Angew. Chem., Int. Ed.* **52**, 1253-1256 (2013).

56. Jiang, S. *et al.*, Porous organic molecular solids by dynamic covalent scrambling. *Nat Commun* **2**, 207 (2011).

57. El-Kaderi, H. M. *et al.*, Designed synthesis of 3D covalent organic frameworks. *Science* **316**, 268-272 (2007).

58. Koenig, S. P., Wang, L., Pellegrino, J., & Bunch, J. S., Selective molecular sieving through porous graphene. *Nat. Nano.* **7**, 728-732 (2012).

59. Nair, R. R. *et al.*, Unimpeded Permeation of Water Through Helium-Leak–Tight Graphene-Based Membranes. *Science* **335**, 442-444 (2012).

60. Kim, H. W. *et al.*, Selective Gas Transport Through Few-Layered Graphene and Graphene Oxide Membranes. *Science* **342**, 91-95 (2013).

Acknowledgements
This work was financially supported by the Engineering and Physical Sciences Research Council (EPSRC, UK), European Research Council (ERC), and an NPRP grant from the QNRF (Qatar). Q.S. acknowledges a PhD scholarship supported by the China Scholarship Council (CSC). S.C. acknowledges a PhD scholarship funded by the Cambridge Overseas Trust. We acknowledge the help from Dr. Wei Li for the nanoindentation measurements. The authors are grateful to the support from the Supercomputing Center of the Chinese Academy of Sciences.

Author contributions
Q.S. and E.S. conceived and designed the research. Q.S. performed all the experiments, analyzed the data and wrote the paper; S.C. contributed to low-pressure gas sorption and data analysis; R.H.P. contributed to stretching measurements; B.G. helped with some gas permeation tests. S.A.A. contributed to industrial application input; E.M.T. and A.K.C. provided facility support and new insights into the research; E.S. guided the project and contributed to writing the paper. All authors discussed the results and commented on the manuscript at all stages.

Additional information
Supplementary information is available in the online version of the paper. Reprints and permissions information is available online at www.nature.com/reprints. Correspondence and requests for materials should be addressed to E.S.

Competing financial interests
The authors declare no competing financial interests.

Figure Legends

Figure 1. Polymer molecular sieves. (**a**) An ideal molecular model of a polymer of intrinsic microporosity (PIM-1) polymer chain segment. (**b**) Three-dimensional view of an amorphous cell of PIM-1 polymer (four polymer segments inside, each containing 10 repeating units). Cell size: 31.8×31.8×31.8 Å, apparent bulk density of 1.050 g cm^{-3}. The grey surface indicates the van der Waals surface, green surface is the Connolly surface with probe radius of 1.65 Å. Dashed circles indicate the bottlenecks between interconnected cavities. (**c, d**) Two-dimensional schematic illustration of thermal oxidative crosslinking of (**c**) independent rigid polymer chains (black contorted lines) to (**d**) covalently crosslinked polymer network *via* thermal treatment at suitable temperature (350-450°C) in the presence of trace amount of oxygen molecules. (**e**) Two-dimensional schematic illustration of pore topologies in microporous polymer membranes and (**f**) thermal-oxidatively crosslinked polymer membranes with narrower or closed gate (indicated by dashed circles) between interconnected cavities, which give better size and shape selectivity (for example, separation of CO_2 from CH_4). White regions indicate the accessible free volume, grey regions indicates the inaccessible pore walls (occupied by polymer chains). (**g**) The upper bound plot of selectivity *versus* permeability for conventional dense polymeric membranes, and microporous molecular sieving membranes, as represented by amorphous PIMs and ordered molecular sieves (MOFs and zeolites) illustrated in inset (**h**). The upper bounds were summarized by Robeson in 1991[16] and 2008[17], respectively.

Figure 2. Characterization of polymer membranes. (**a**) Photo of PIM-1 polymer solution in chloroform. (**b**) Photo of as-prepared PIM-1 membrane. (**c**) Photo of thermal-oxidatively crosslinked (TOX) PIM-1 membrane, and (**d**) solubility test in chloroform. (**e**) Stress-strain curve of PIM-1 and TOX-PIM-1 membranes. (**f**) Thermogravimetric analysis of PIM-1 polymer membranes in argon (black), 200 ppm O_2 in argon (blue), and air (red). Samples were heated to 1000°C at 10°C min^{-1}, and (**g**) corresponding *in situ* FTIR spectra of gaseous products in argon atmosphere. (**h**) Weight loss profiles of isothermal oxidative degradation of PIM-1 membranes in 200 ppm O_2/argon, in the temperature range of 300-450°C (full profiles are shown in Supplementary Fig. 10). (**i**) Photos of polymer films after isothermal oxidative crosslinking in 200 ppm O_2/argon for 2 h at temperatures corresponding to (**h**). (**j**) Molecular weight distribution of soluble fraction of TOX-PIM-1 polymer membranes. (**k**) Gel content analysis and peak molecular weight of soluble fraction. The polymer membranes were heated at 385°C under continuous vacuum (1 mbar) up to 24 h.

Figure 3. Gas sorption and transport properties. (**a**) N_2 adsorption-desorption isotherms at 77 K. (**b**) Gas sorption isotherms at 273 K and (**c**) high-pressure gas sorption at 295 K (open symbols: PIM-1 membrane; solid symbols: TOX-PIM-1 membrane). (**d**) Permeability *versus* kinetic diameter of gases measured at 295 K. (**e**) Gas solubility (1 bar, 295 K) as a function of critical temperature (T_C) of gas molecules. (**f**) Diffusivity as a function of square of effective molecular diameter (d_{eff}) of gas molecules at 295 K. (**g**) Robeson plot of CO_2/CH_4 selectivity *versus* CO_2 permeability**.** Commercial polymers are included for comparison: cellulose acetate (CA); ethyl cellulose (EC); polycarbonate (PC); Matrimid® 5218 polyimide (PI); polyetherimide (PEI); polyphenyleneoxide (PPO); polysulfone (PSF), cited from reference are included for comparison[40]. Upper bound line: Robeson upper bound (2008)[17]. Open squares: PIM-1 in literature; solid triangles: other PIMs in literature[21,32-34,41], TZ-PIM[20], PIM-SBF[32], PIM-EA-TB[21], and PIM-SBI-TB[21]; Open circles: TR polymers[18,31,34,42-44]; Solid squares (black): unmodified PIM-1; Solid squares (red): TOX-PIM-1 membranes. (**h**) CO_2/CH_4 selectivity and (**i**) CO_2/N_2 selectivity *versus* the fugacity of CO_2 for separation of gas mixtures (50/50 vol.%). The unmodified dense PIM-1 polymer membrane was annealed at 120°C for 24 h under vacuum. The TOX-PIM-1 membrane in all panels was thermal-oxidatively crosslinked at 385°C for 24 h under vacuum (1 mbar), the same condition as the sample shown in Fig. 2c.

Figure 4. Tunable gas transport properties. (**a**) Permeability and (**b**) selectivity as a function of annealing temperature under vacuum (1 mbar). All samples were thermally treated at set-point temperature for 24 h under vacuum, except that the sample at 400°C was annealed for 12 h. (**c**) Permeability and (**d**) selectivity of PIM-1 membranes exposed to heat treatment at 385°C under vacuum (1 mbar) for varied periods. (**e**) Permeability and (**f**) selectivity of membranes exposed to heat treatment at 385°C in purging gas of argon containing ppm-level

O_2. More data are given in Supplementary Table 3. (**g**) Robeson upper bound plot of CO_2/CH_4 selectivity versus CO_2 permeability showing the trend of gas transport properties upon exposure to thermal oxidative crosslinking. Arrows are added to guide the eyes. Data sets also include TR polymers by Park *et al*[18], and thermally crosslinked PIM-1 membranes by Li et al[36]. (**h**) Change of gas transport properties of TOX-PIM-1 membranes under vacuum over 330 days. TOX-PIM-1 membrane was prepared by thermal-oxidative crosslinking at 385°C in argon containing 10 ppm O_2. (**i**) Robeson plot showing the aging of PIM-1 (about 450 days) and TOX-PIM-1 membranes (about 330 days). Detailed data are given in Supplementary Fig. 17. Sample (1) and (2) correspond to membranes exposed to heat treatment at 385°C for 24 h in argon containing 10 ppm and 100 ppm O_2, respectively.

Figure 5. Upper bound plot. Selectivity *versus* permeability of PIM-1 and TOX-PIM-1 membranes for industrially important gas pairs. (**a)** H_2/CH_4, (**b**) H_2/N_2 (**c**) O_2/N_2, and (**d**) CO_2/N_2. Red lines: State-of-the-art upper bound of polymer membrane summarized by Robeson in 2008[17]. Commercial polymers (grey regions) are included for comparison. Open squares: PIM-1 in literature; Solid triangles (yellow regions): other PIMs in literature[21,32-34,41]; Open circles: TR polymers[18,31,42-44]; Solid squares (black): PIM-1 membrane; Solid squares (red): representative TOX-PIM-1 membranes under different thermal oxidation conditions (detailed data are given in Supplementary Table 3).

Figure 1

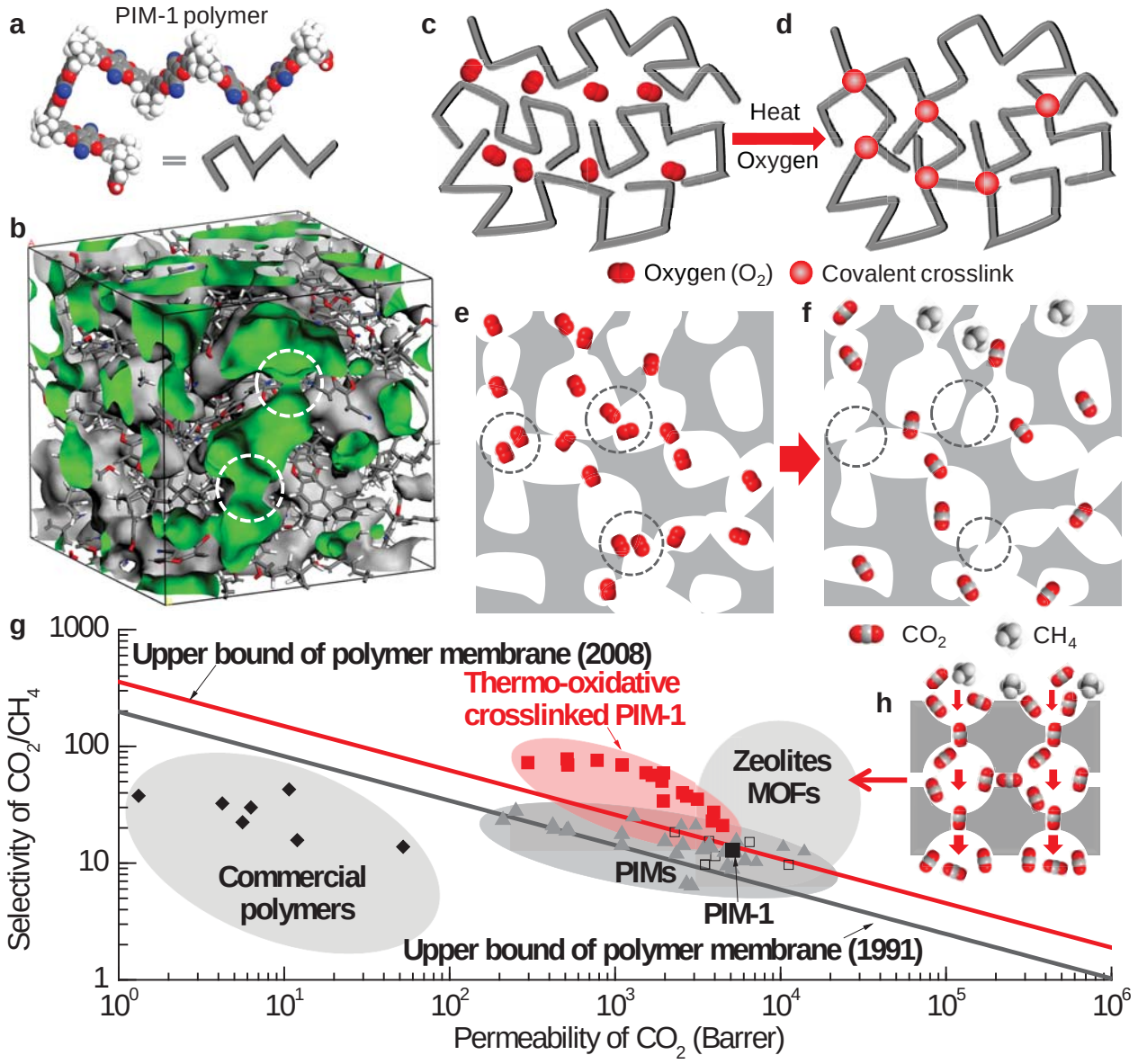

Figure 2

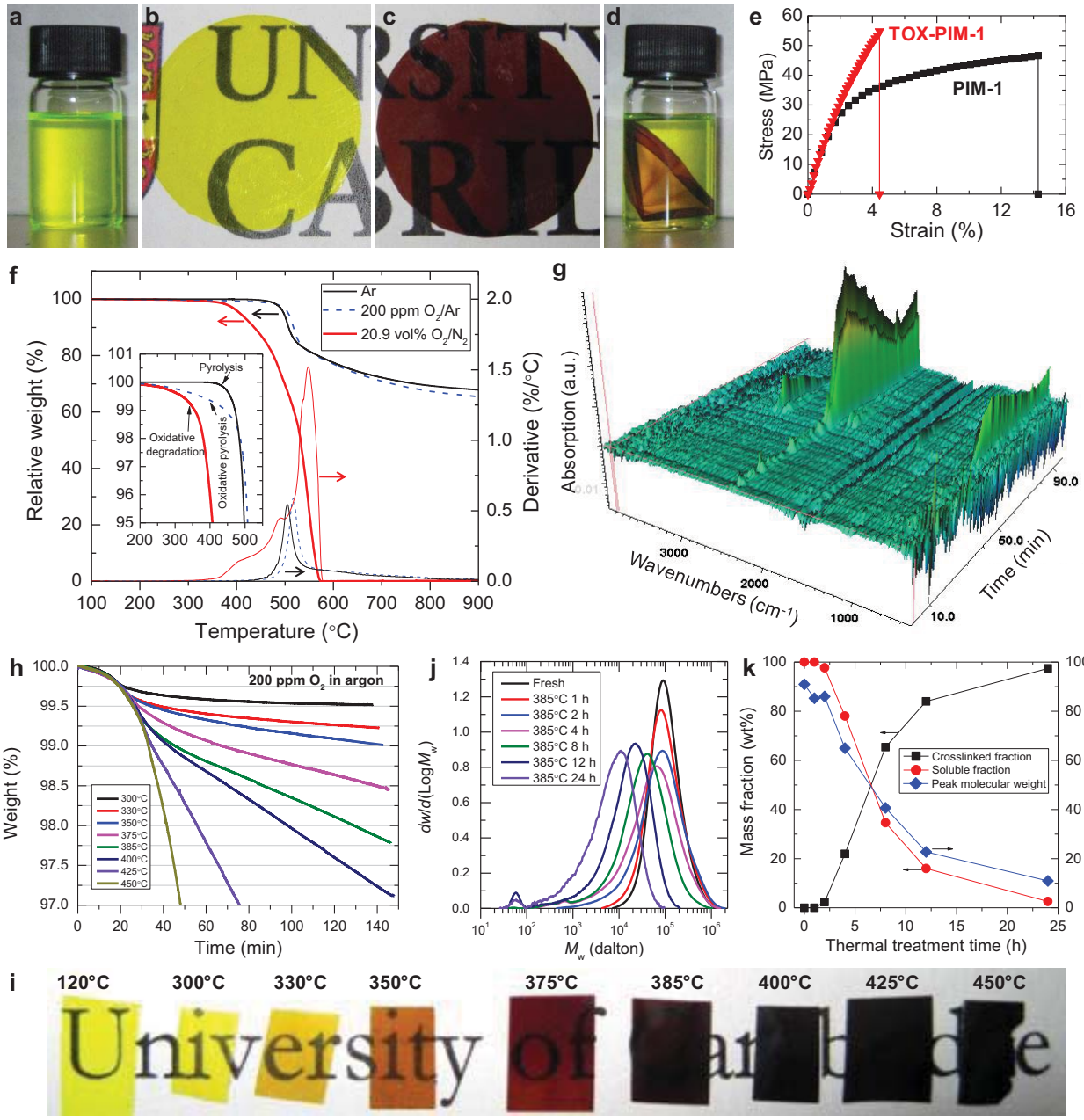

Figure 3

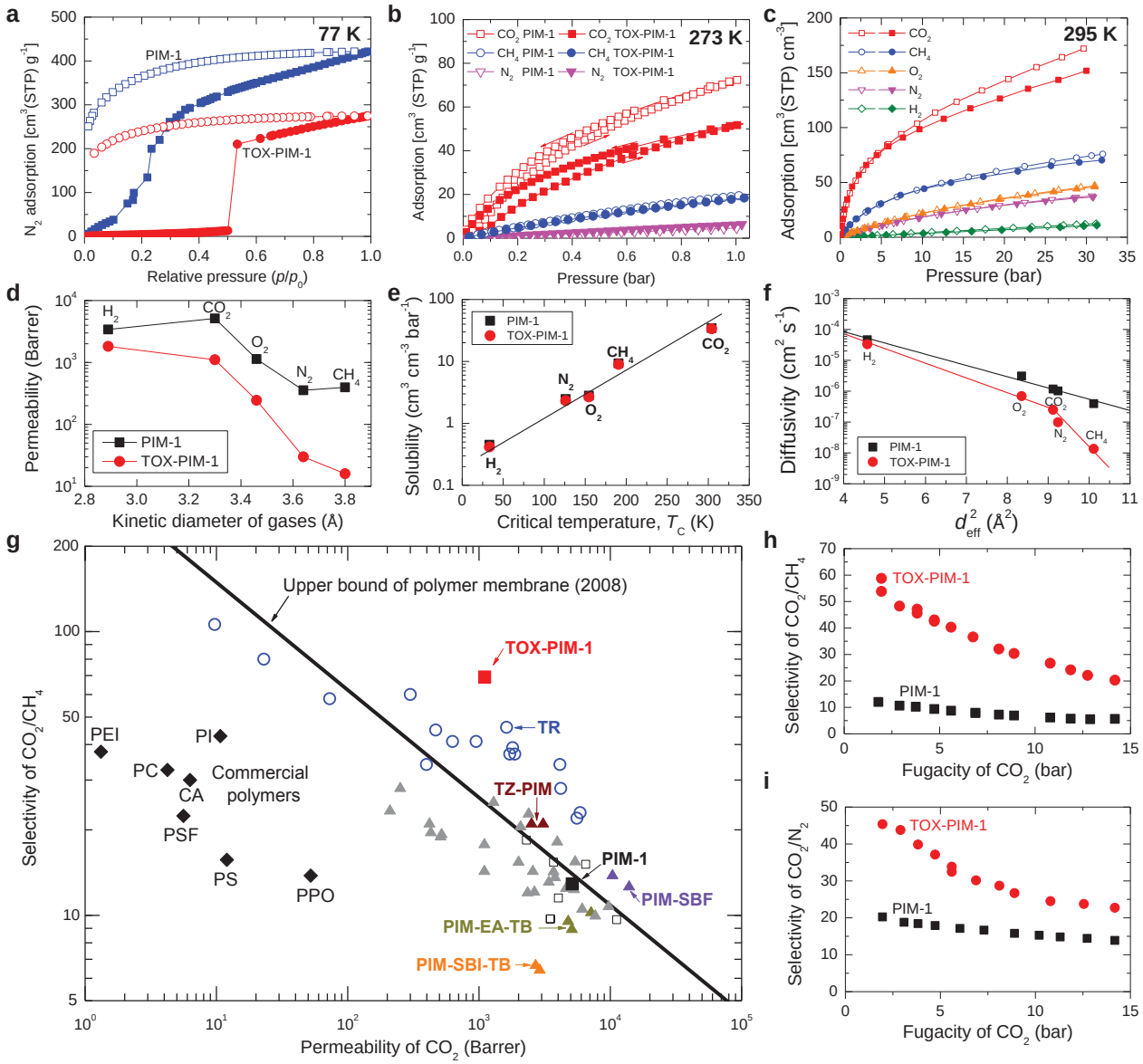

Figure 4

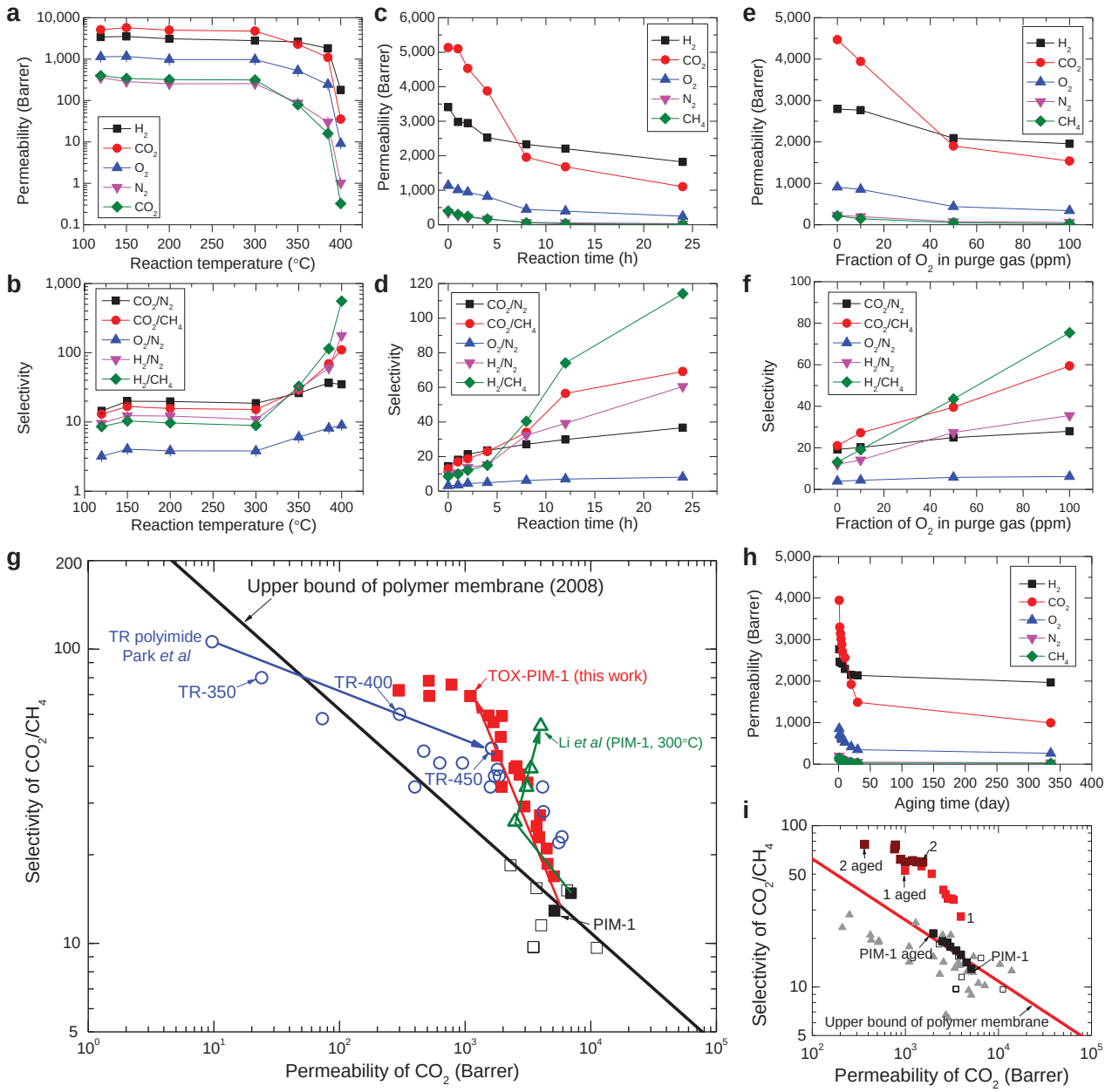

Figure 5

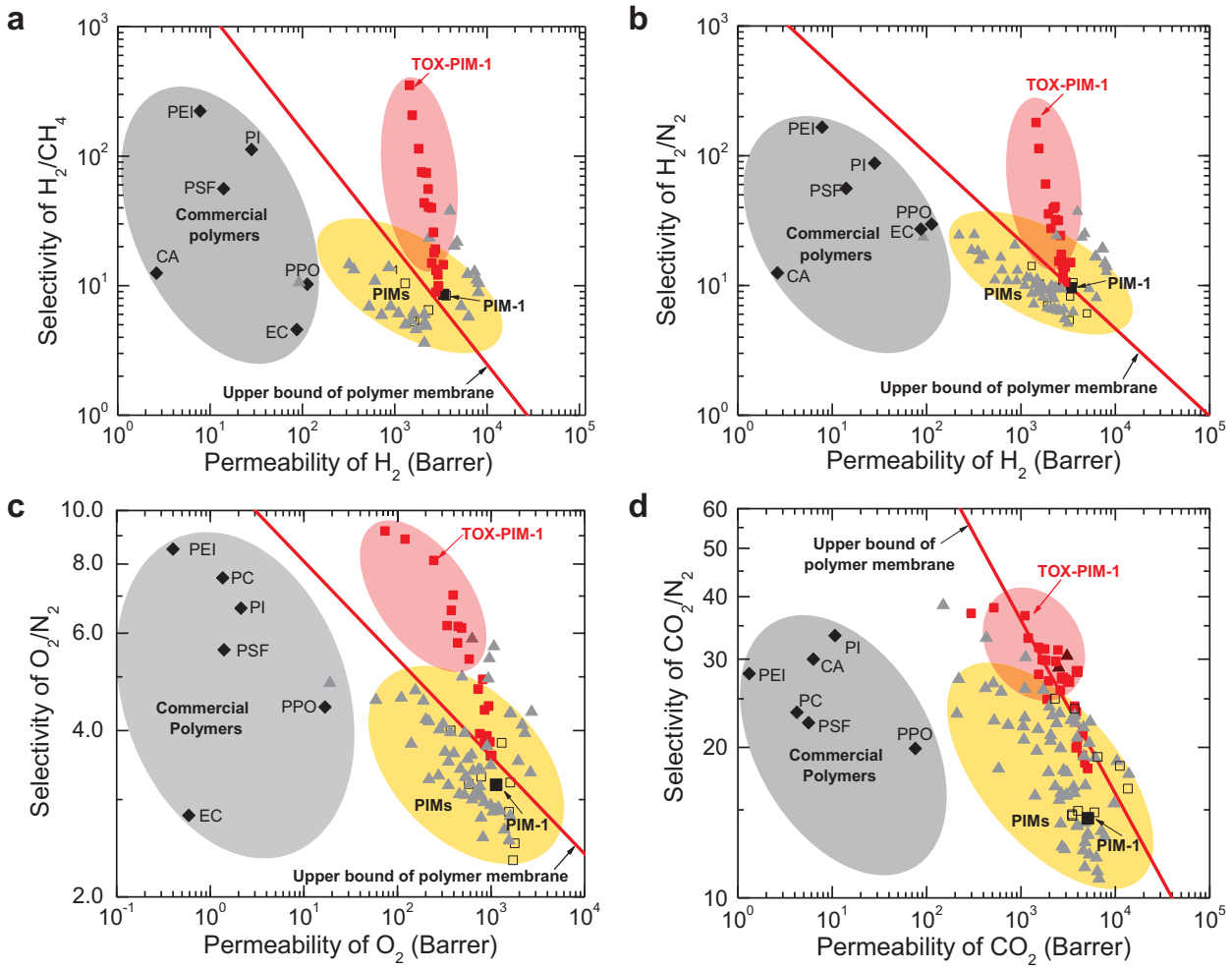

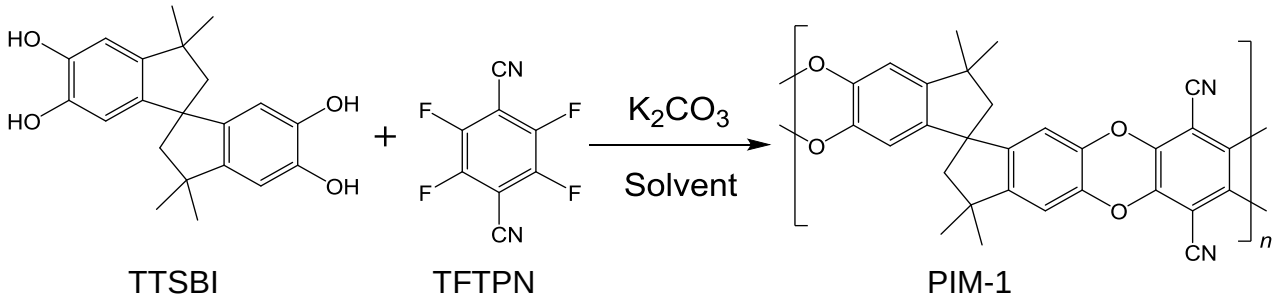

TTSBI TFTPN PIM-1

Supplementary Figure 1: Synthesis of PIM-1 polymer. TTSBI: 5,5′,6,6′-tetrahydroxy-3,3,3′,3′-tetramethylspirobisindane; TTFPN: 2,3,5,6-tetrafluoroterephthalonitrile; Solvent was dimethylformamide.

Supplementary Figure 2: Solubility tests. Solubility of fresh PIM-1 (1) and thermally crosslinked PIM-1 membranes in common solvents (2-20). (1) Chloroform, (2) Chloroform (94.1wt%), (3) Tetrahydrofuran (92.6wt%), (4) Dichloromethane (95.1wt%), (5) Chlorobenzene (98.9wt%), (6) 1,2 Dichlorobenzene (99.4wt%), (7) N-Methyl-2-pyrrolidone (NMP) (96.9wt%), (8) Dimethylformamide (DMF) (97.6wt%) (9) 1,4 Dioxane (98.8wt%), (10) Acetone (99.0wt%) , (11) Dimethyl sulfoxide (DMSO) (99.0wt%), (12) Toluene, (13) Hexane, (14) Cyclohexane, (15) Acetic acid, (16) Isopropanol, (17) Ethanol, (18) methanol, (19) Diluted HCl, 32%, (20) NaOH (20wt%) in water. The gel content of crosslinked PIM-1 membranes after swelling in these solvents are marked in the parentheses. For solvent 12-20, the gel content is about 100wt%. Prior to exposure to solvent, the crosslinked polymer films were heated at 120 ℃ under vacuum for overnight to remove the moisture and with the mass measured immediately. The insoluble film or gel was removed from the solution by filtration or by centrifugation, washed with methanol and dried under vacuum at suitable temperature (depending on the solvent). After, the mass was recorded again to quantify the content of crosslinked part. The solution containing dissolved polymer in chloroform was used for GPC measurements to quantify the evolution of molecular weight distribution.

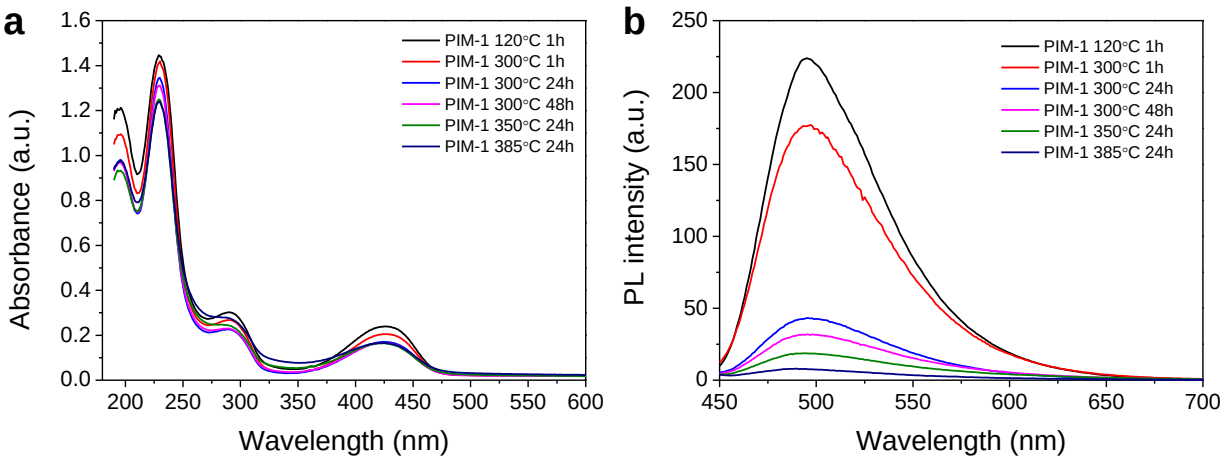

Supplementary Figure 3: Optical properties. (**a**) UV-vis absorption spectra and (**b**) photoluminescence spectra of PIM-1 thin films thermally treated at different conditions. Thin films were prepared by spin-coating of diluted PIM-1 polymer solution in chloroform (0.8 wt%) on quartz glass substrate, at speed of 2000 rpm with an acceleration speed of 1500 rpm. The thermal treatment was performed in the high-temperature vacuum oven, the same batch as the thermal treatment of dense polymer membranes. The mechanism of fluorescence is not fully understood, however, the loss of photoluminescence clearly indicates the degradation.

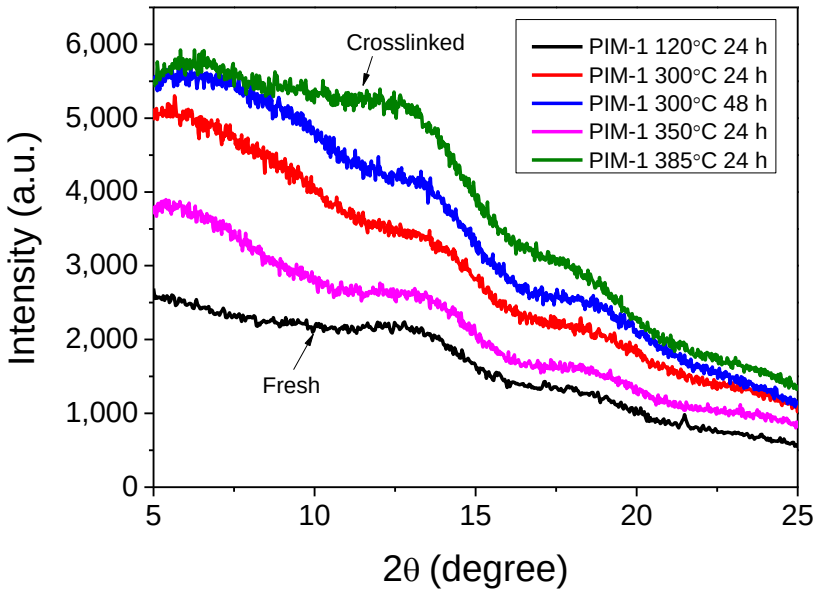

Supplementary Figure 4: Wide angle X-ray scattering. PIM-1 polymer films after exposure to thermal treatment under vacuum of 1 mbar.

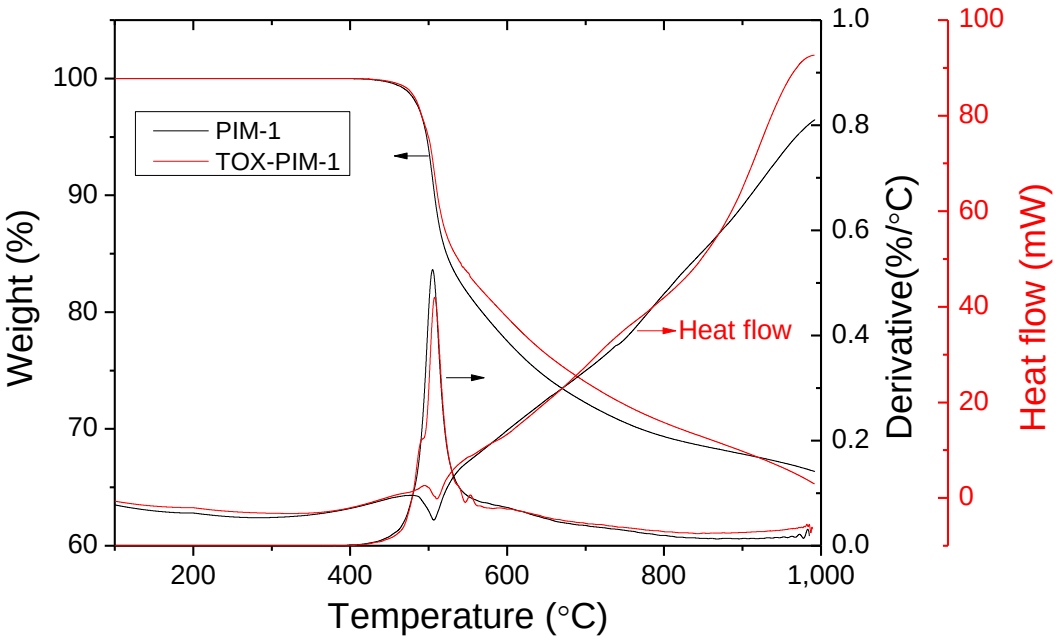

Supplementary Figure 5: Thermal stability in inert atmosphere. TGA/DSC analyses of fresh PIM-1 and thermo-oxidative crosslinked (TOX) PIM-1 polymer membranes in argon, at a heating rate of 10 ℃ min^{-1}. The TOX-PIM-1 membrane was heated at 385 ℃ for 24 h under vacuum of 1 mbar.

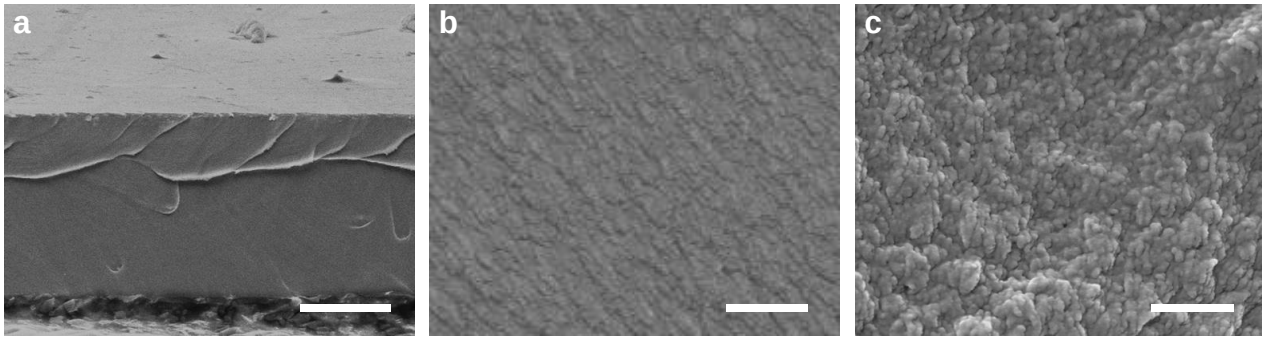

Supplementary Figure 6: Cross-sectional SEM images of polymer films. (**a**) Thick PIM-1 polymer film and (**b**) enlargement. (**c**) Cross-section of TOX-PIM-1 polymer film. Scale bar: (**a**) 20 µm, (**b, c**) 200 nm. The TOX-PIM-1 membrane was cured at 385 ℃ for 24 h under vacuum of 1 mbar.

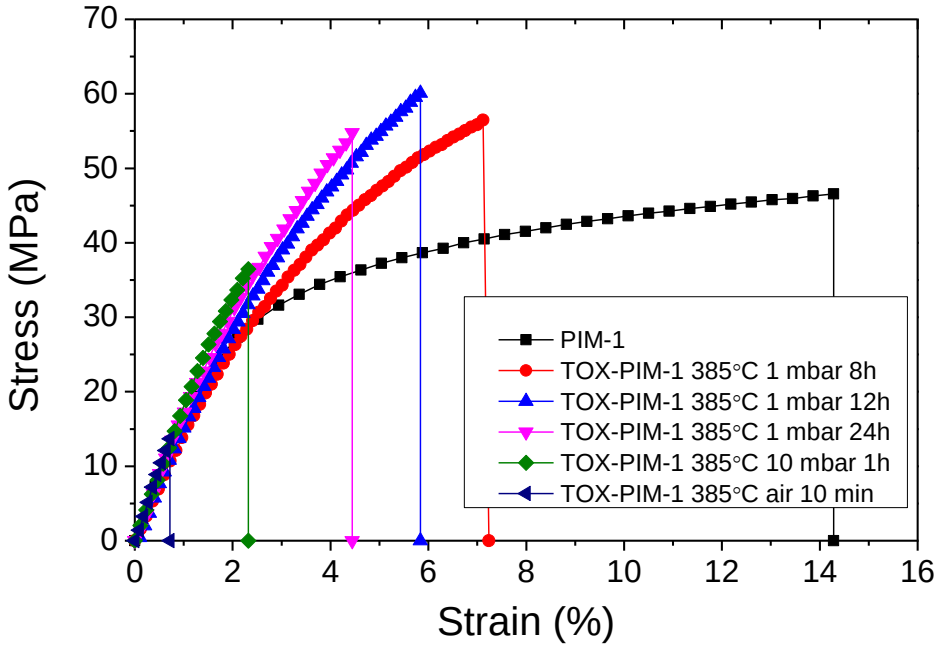

Supplementary Figure 7: Stress-strain curves. Thick PIM-1 polymer films (~50 μm) were exposed to thermal oxidative degradation at 385 ℃ under vacuum for varied time. In extreme case, the polymer film was exposed to heat treatment at 385 ℃ in air for 10 min.

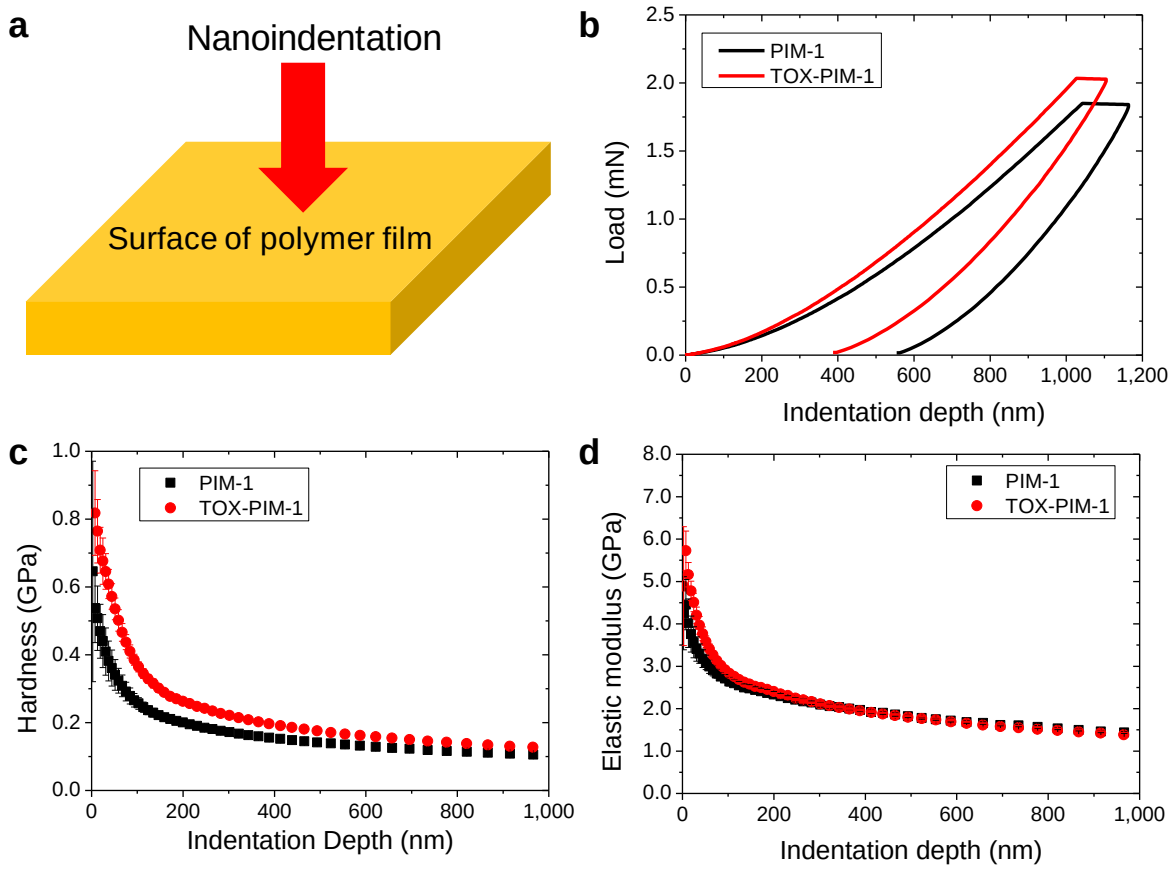

Supplementary Figure 8: Nanoindentation. (**a**) Schematic diagram of nanoindentation of membrane surface. (**b**) Load-displacement curves of PIM-1 (black) and thermally crosslinked dense TOX-PIM-1 (red) membranes (~50 μm). (**c**) Hardness as a function of displacement (indentation depth). (**d**) Elastic modulus as a function of displacement.

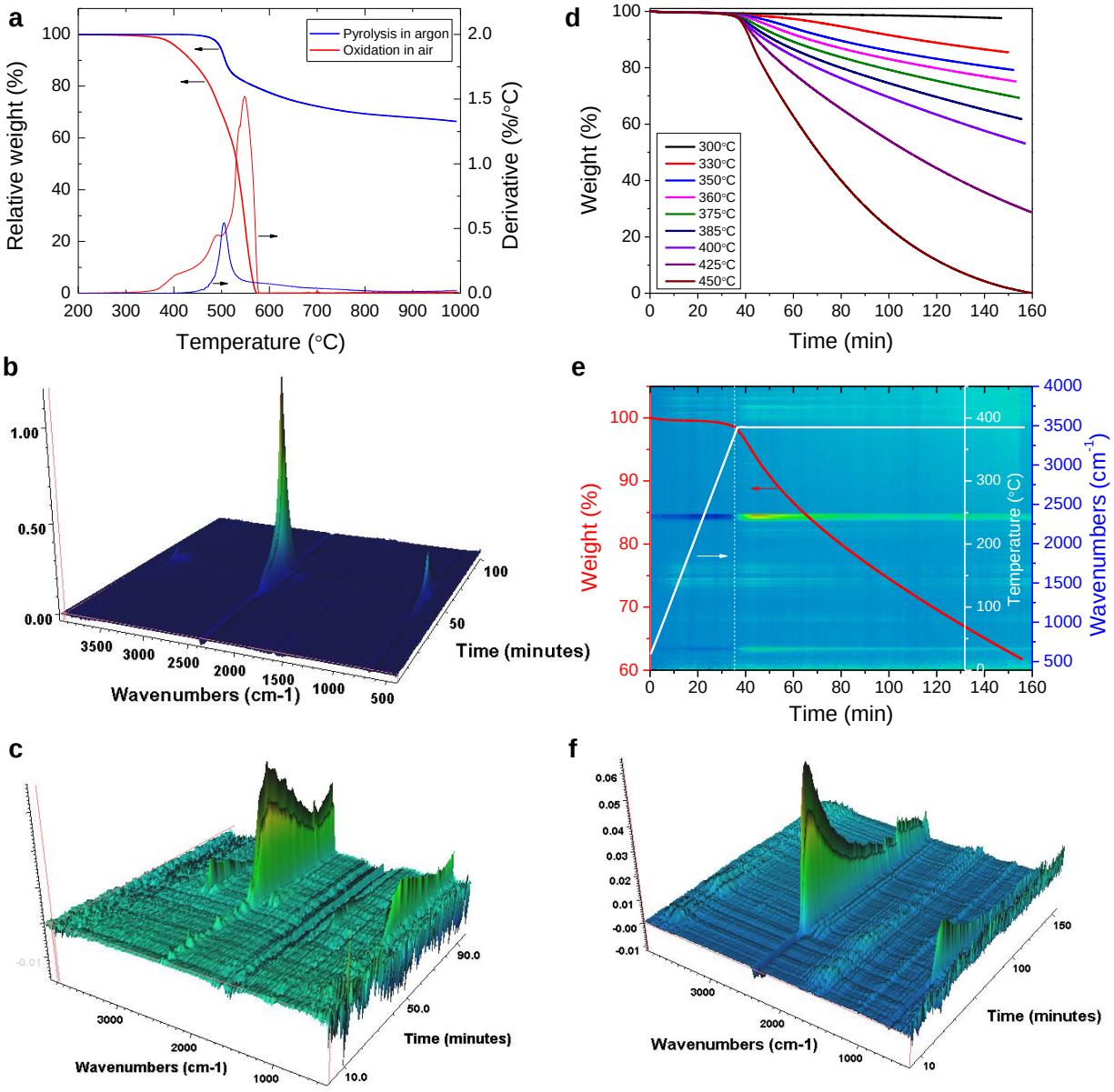

Supplementary Figure 9: Thermogravimetric analyses. (**a**) Thermal degradation under purging gas of air (oxidation, red lines) and argon (pyrolysis, blue lines), and FTIR spectra of evolved gaseous products under purging gas of air (**b**) and argon (**c**). (**d**) Isothermal degradation over 300-450 ℃. (**e**) Isothermal degradation at 385 ℃ and (**f**) 3D FTIR spectra of evolved gaseous products. For dynamic thermal analysis (**a-c**), the polymer films were heated from room temperature to 1000 ℃ at 10 ℃ min^{-1}. For isothermal analysis (**d-f**), the polymer films were heated from room temperature to set-point temperature at 10 ℃ min^{-1}, and then maintained for 120 min.

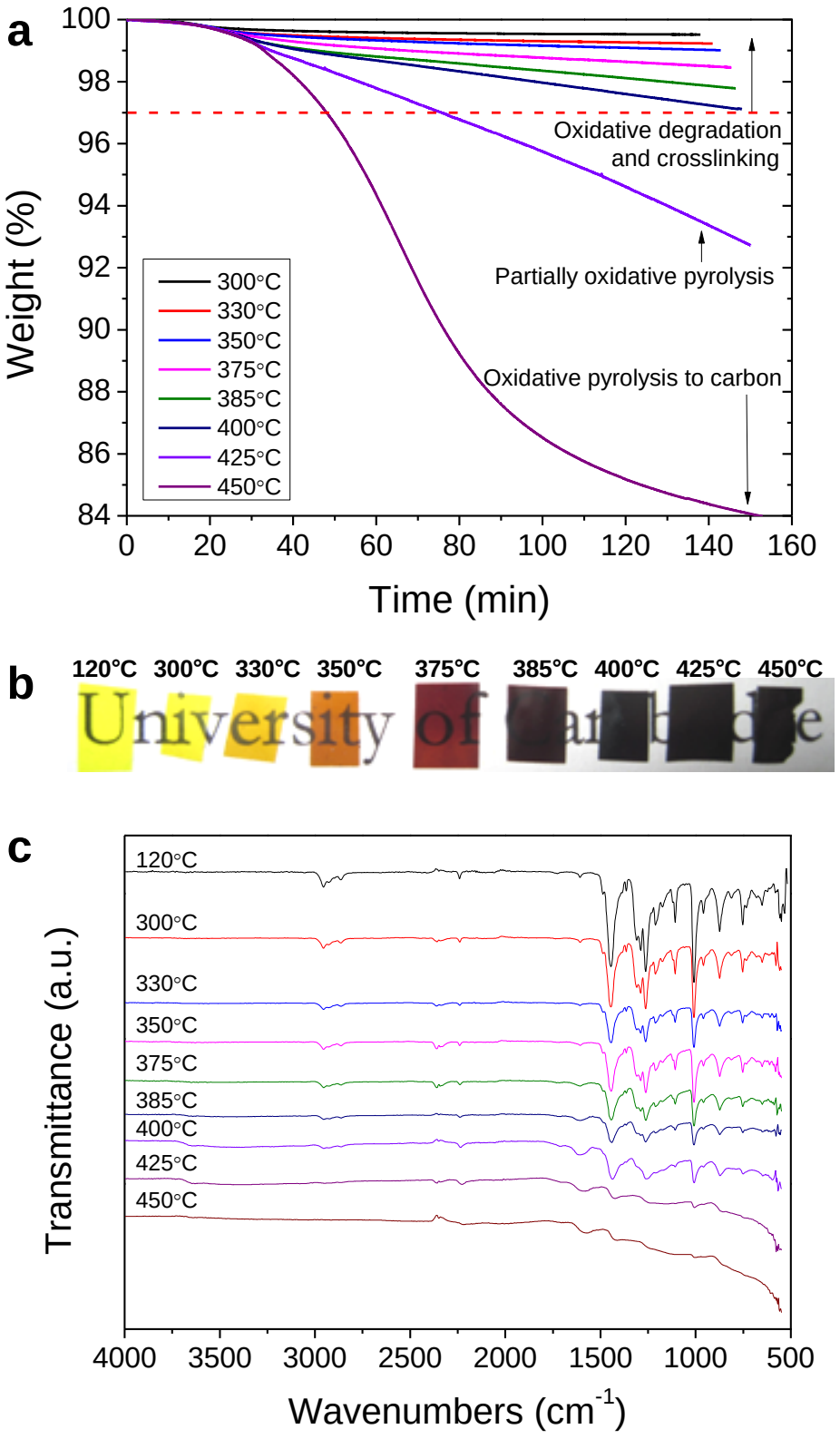

Supplementary Figure 10: Thermal oxidative degradation and *ex situ* FTIR spectra of polymer films. (**a**) Isothermal TGA analyses of PIM-1 polymer films over 300-450 ℃ in 200 ppm O_2 in argon. (**b**) Photos of membranes after exposure to thermal degradation corresponding to (**a**). (**c**) FTIR-ATR spectra of polymer films after isothermal TGA analyses.

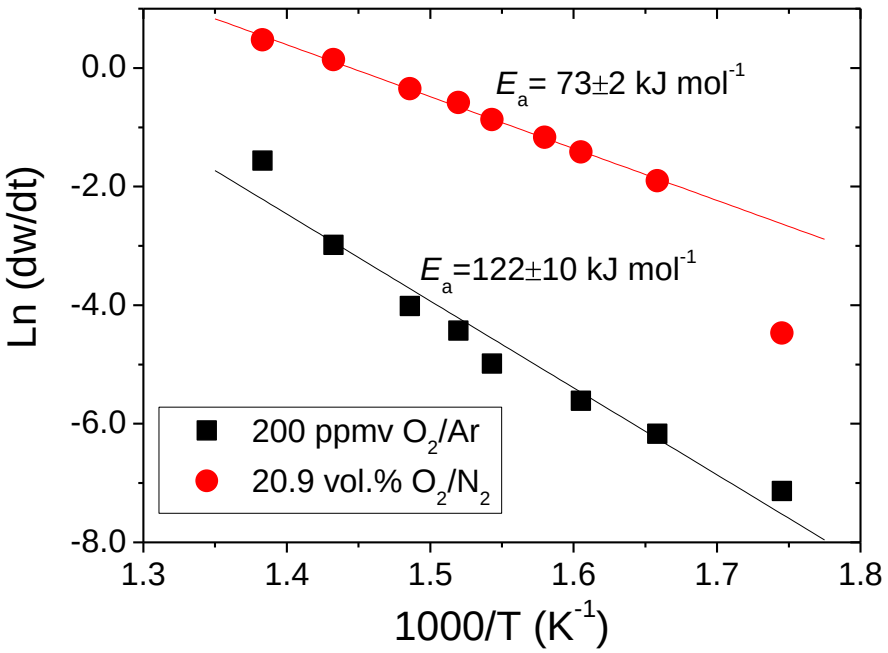

Supplementary Figure 11: Arrhenius plot of rates of oxidative degradation *versus* temperature. Squares: 200 ppm O_2/Argon, Circles: 20.9 % O_2/N_2. The reactions rates were derived from linear fitting of the isothermal weight loss stage in Supplementary Figures 8d and 9a.

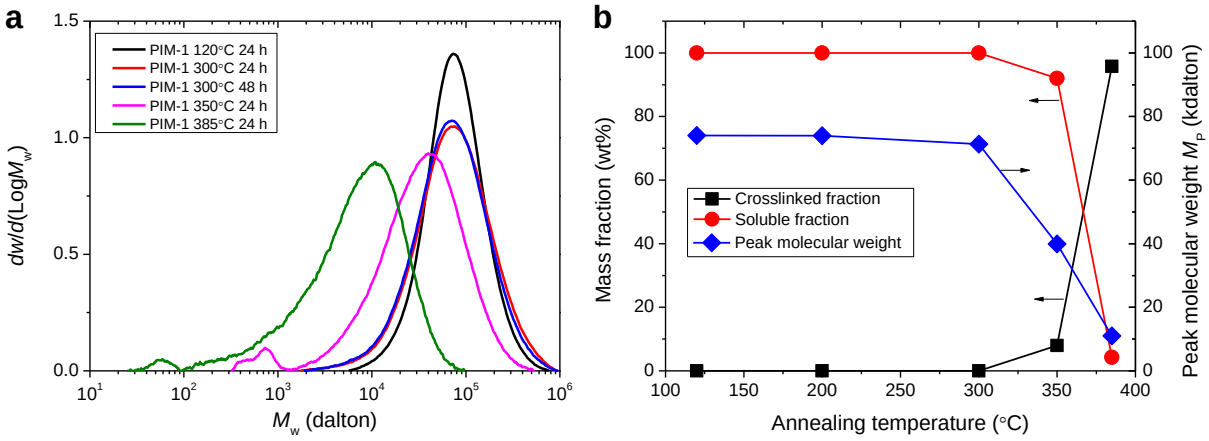

Supplementary Figure 12: Molecular weight distribution and gel content evolution. (**a**) Molecular weight distributions of soluble fractions of PIM-1 polymer membranes after exposure to thermal oxidative treatment under vacuum (1 mbar) at varied temperatures. (**b**) Gel content analysis and peak molecular weight of soluble fractions of PIM-1 polymer membranes.

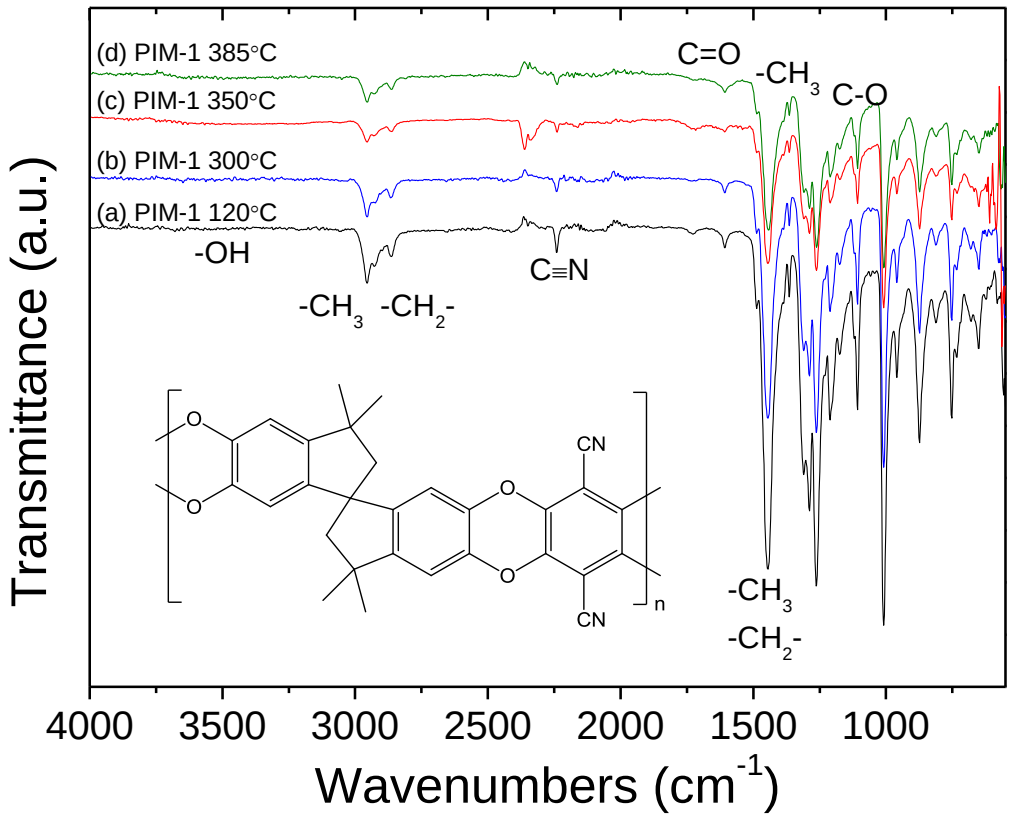

Supplementary Figure 13: *Ex situ* FTIR spectra of PIM-1 polymer membranes. All samples were annealed under vacuum (1 mbar) for 24 h, except that the samples at 300 ℃ were annealed for 48 h.

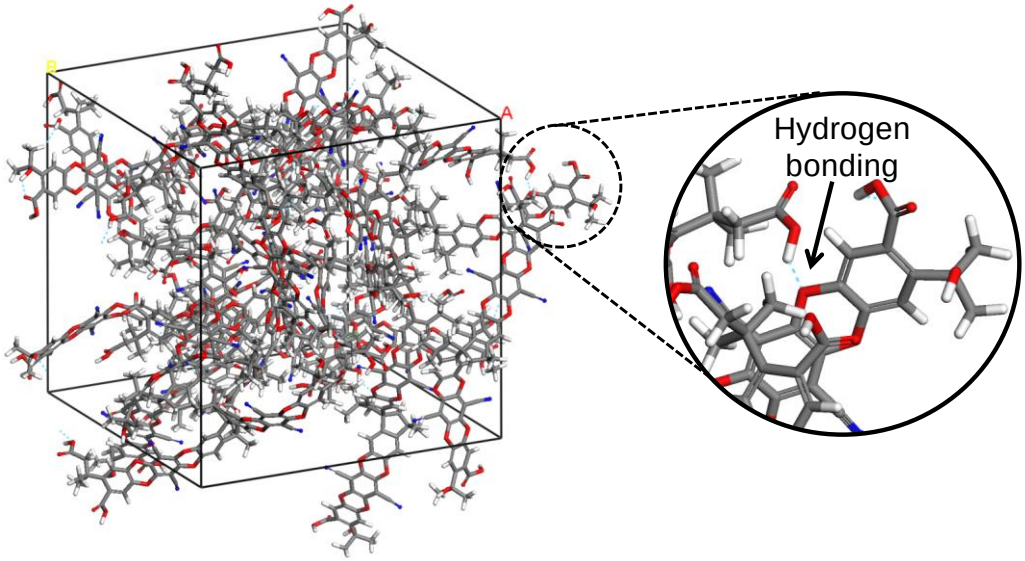

Supplementary Figure 14: Hydrogen-bonded networks. Three-dimensional molecular simulation of an amorphous cell with 20 short polymer chain segments with two PIM-1 repeating units and capped with –COOH groups, to mimic the shorter polymer chains due to thermal oxidative chain scission. Cell size: 31.7×31.7×31.7 Å, density: 1.174 g cm^{-3}. Enlargement shows the possible intermolecular interactions *via* hydrogen bonding (blue dotted line) between ether linkages of the backbone and hydroxyl-containing groups (carboxylic acid) of oxidized polymer segments. Intermolecular covalent crosslinking is not considered here. Carbon: black; Oxygen: red; Hydrogen: grey; Nitrogen: blue.

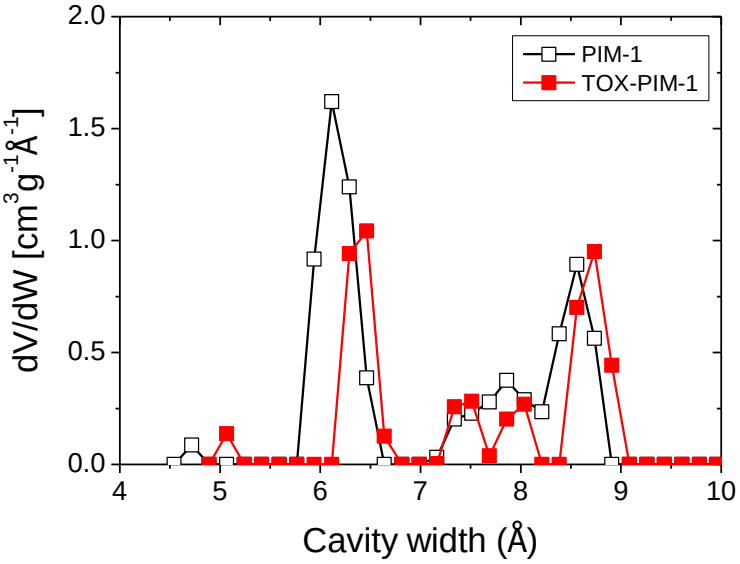

Supplementary Figure 15: Pore size distribution. The data were derived from CO_2 sorption isotherms at 273 K (Fig. 4b) based on non-local density functional theory (NLDFT) method. Dense PIM-1 membrane was annealed at 120 ℃ under vacuum. The TOX-PIM-1 membrane was thermo-oxidatively crosslinked at 385 ℃ for 24 h under vacuum (1 mbar). The apparent loss of ultramicroporosity (size smaller than 7 Å) seems to agree with our proposed mechanism of narrower bottlenecks of the interconnected micropores.

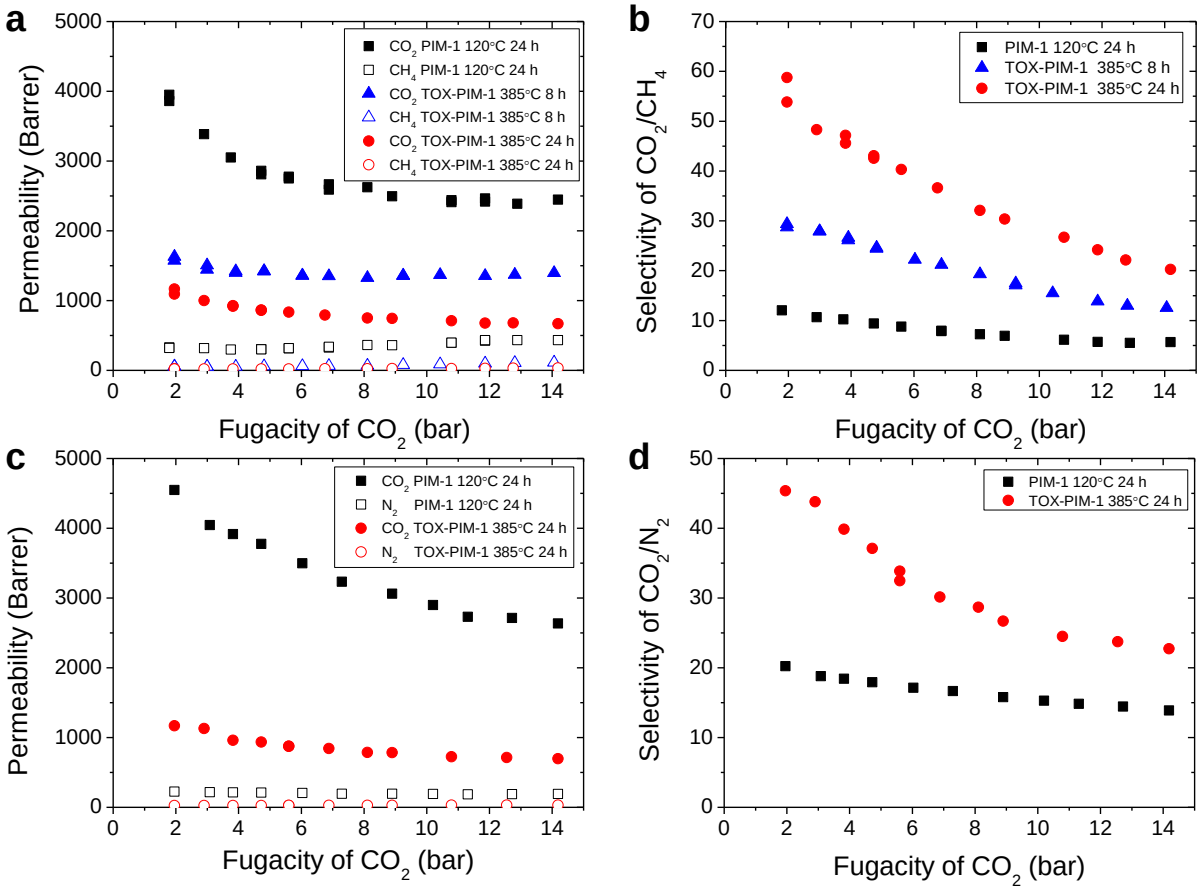

Supplementary Figure 16: Mixed gas transport properties. Permeability and selectivity of PIM-1 and TOX-PIM-1 membranes for (**a-b**) CO_2/CH_4 mixture and (**c-d**) CO_2/N_2 mixture.

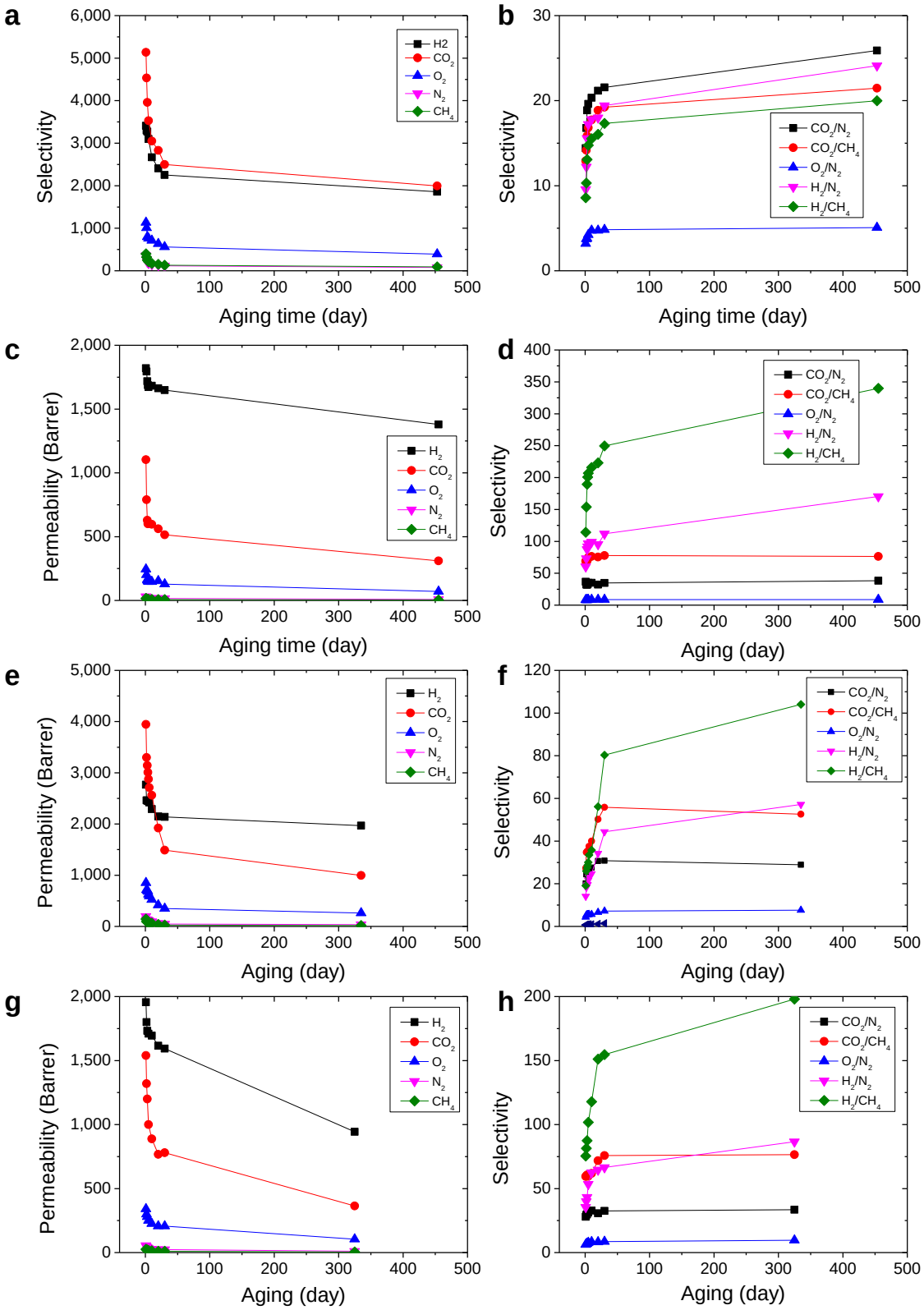

Supplementary Figure 17: Aging of gas transport properties. (**a, b**) Unmodified PIM-1 membrane. (**c, d**) TOX-PIM-1 membranes heated at 385 ℃ for 24 h under vacuum (1 mbar). (**e, f**) TOX-PIM-1 membranes heated at 385 ℃ under 10 ppm O_2 in argon for 24 h. (**g, h**) TOX-PIM-1 membrane heated at 385 ℃ under 100 ppm O_2 in Argon for 24 h. The membranes were kept under vacuum between gas permeation measurements.

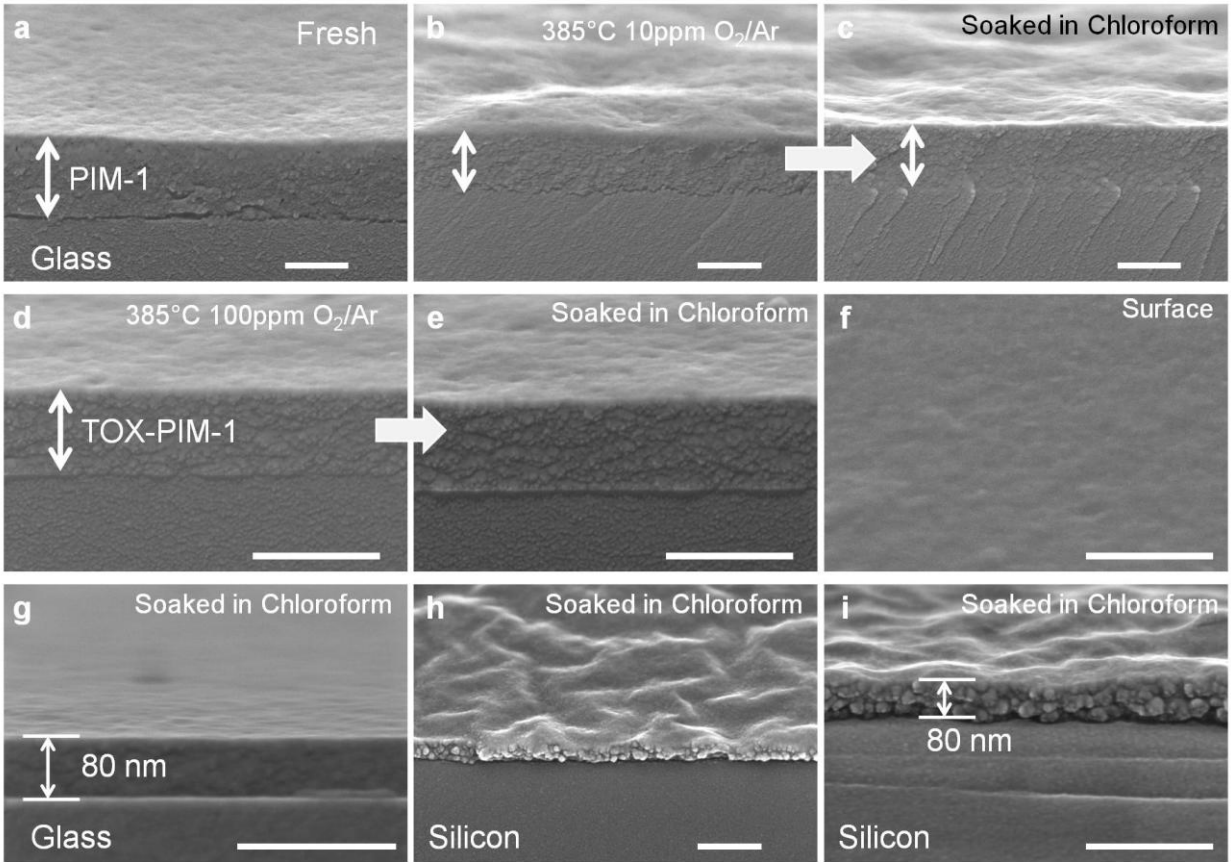

Supplementary Figure 18: Cross-sectional SEM images of polymer thin films. (**a**) Fresh as casted PIM-1 film. (**b**) TOX-PIM-1 at 385 ℃ for 24 h under continuous purging gas of 10 ppm O_2 in argon, and (**c**) soaked in chloroform for 24 h. (**d**) TOX-PIM-1 thin film at 385 ℃ for 24 h under continuous purging gas of 100 ppm O_2 in argon, and (**e**) further soaked in chloroform for 24 h, and (**f**) surface. TOX-PIM-1 thin films (**g-i**) at 385 ℃ for 24 h under vacuum of 1 mbar, and soaked in chloroform for 24 h. Polymer thin films were formed by spin-coating diluted solution on (**a-g**) glass substrate and (**h-i**) silicon wafer. (**a-f**) Films were spin-coated with 2wt% polymer solution in chloroform at 2000 rpm with an acceleration speed of 1500 rpm, giving an initial thickness of ~250 nm. (**g-i**) Films were spin-coated with 0.8 wt% polymer solution in chloroform at 2000 rpm with an acceleration speed of 1500 rpm, giving an initial thickness of ~100 nm. Scale bar in all panels: 200 nm.

Supplementary Table 1. Mechanical properties. The data were derived from stress-strain profiles of PIM-1, thermal-oxidatively crosslinked PIM-1 films, and some representative membranes in the literature.

Samples	Tensile strength at break (MPa)	Elongation Strain at break (%)	Young's modulus (GPa)	reference
PIM-1	47.5 ±2.3	14.3	1.43 ±0.15	This work
TOX-PIM-1 385 ℃ 1 mbar 8 h	56.5 ±2.8	7.1	1.28 ±0.37	This work
TOX-PIM-1 385 ℃ 1 mbar 12 h	60.0 ±3.0	5.8	1.45 ±0.05	This work
TOX-PIM-1 385 ℃ 1 mbar 24 h	54.8 ±2.7	4.4	1.72 ±0.05	This work
TOX-PIM-1 385 ℃ 10 mbar 1 h	36.4 ±1.8	2.3	1.80 ±0.02	This work
TOX-PIM-1 385 ℃ air 10 min	14.0 ±0.7	0.7	1.96 ±0.03	This work
Literature				
PIM-1	47.8	10.0	n.a.	1
PIM-EA-TB	-	-	0.80	2
spiroTR-PBO-6F	82.3 ±1.3	20.0 ±4.0	n.a.	3
spiroTR-PBO-PM	79.2 ±3.5	17.3 ±3.6	n.a.	3
spiroTR-PBO-BP	94.4 ±1.4	14.9 ±0.5	n.a.	3
spiroTR-PBO-BPA	69.9 ±4.4	19.7 ±0.2	n.a.	3
TR- PIOFG-1-350	87	3.8	n.a.	4
TR- PIOFG-1-400	95	3.5	n.a.	4
TR- PIOFG-1-450	98	3.9	n.a.	4
CMS-Kapton polyimide 600 ℃	42	0.4	n.a.	4
CMS-Kapton polyimide 800 ℃	52	0.3	n.a.	4
CMS-PIOFG-1 600 ℃	34	0.6	n.a.	4

Supplementary Table 2. Gas permeability, solubility, and diffusion coefficient for PIM-1 and a representative TOX-PIM-1 membranes (heated at 385 ℃ for 24 h under vacuum of 1 mbar).

Parameters	Pure gas					Gas pairs				
	H_2	CO_2	O_2	N_2	CH_4	CO_2/N_2	CO_2/CH_4	O_2/N_2	H_2/CO_2	H_2/CH_4
Critical temperature T_C (K)	33.2	304.2	154.6	126.3	190.9					
Kinetic diameter (Å)	2.89	3.30	3.46	3.64	3.8					
Effective diameter d_{eff} (Å) [a]	2.14	3.02	2.89	3.04	3.18					
$\boldsymbol{D_K}$ (10^{-8} cm^2 s^{-1})[b]	11780	2510	2950	3150	4160	0.80	0.60	0.94	4.7	2.8
PIM-1										
P (Barrer)	3408	5135	1135	356	397	14.4	12.9	3.2	0.7	8.6
S [cm^3 (STP) cm^{-3} bar^{-1}] [c]	0.452	34.60	2.80	2.47	9.3	14.0	3.7	1.1	0.01	0.05
D (10^{-8} cm^2 s^{-1}) [d]	4647	117	311	102	39	**1.1**	**3.0**	**3.0**	**40**	**119**
TOX-PIM-1										
P (Barrer)	1820	1100	245	30.1	15.9	37	69	8.1	1.7	115
S [cm^3 (STP) cm^{-3} bar^{-1}] [c]	0.42	33.70	2.68	2.33	8.95	14.5	3.8	1.2	0.01	0.05
D (10^{-8} cm^2 s^{-1}) [d]	3317	24.9	69.4	9.8	1.35	**2.5**	**18.4**	**7.1**	**133**	**2457**

[a] reference[5]

[b] Knudsen diffusion coefficient, calculated from equation: $D = d_p\sqrt{8RT/\pi M}/3$, where d_p is the pore diameter (m, here we assume the pore diameter as 2 nm), R is the gas constant (J mol^{-1} K^{-1}), T is the temperature (K), M is the molecular weight of gas molecules (g mol^{-1}).

[c] gas solubility measured at 1 bar at 22 ℃

[d] calculated from $D=P/S$, as the gas permeability is quite constant at low permeation pressure.

Supplementary Table 3. Gas transport properties of TOX-PIM-1 polymer membranes. Batch 1 membranes were thermally treated under vacuum (1 mbar) at varied temperatures. Batch 2 membranes were thermally treated at 385 ℃ under vacuum (1 mbar) for varied reaction time. Batch 3 membranes were thermally oxidized at 385 ℃ under varied vacuum pressure. Batch 4 membranes were thermally treated at 385 ℃ for 1 h under continuous purging gas containing varied concentration of O_2. Batch 5 were thermally crosslinked at 385 ℃ for 24 h under continuous purge gas containing varied concentration of O_2 over 24 h. Note: samples in Batch 4 were based on a separate batch of polymer films with slightly higher initial permeability.

Operation condition	Permeability (Barrer)					Selectivity				
	H_2	CO_2	O_2	N_2	CH_4	CO_2/N_2	CO_2/CH_4	O_2/N_2	H_2/N_2	H_2/CH_4
Batch 1, varied reaction temperature, vacuum of 1 mbar										
120 ℃ 24h	3408	5135	1135	356	397	14.4	12.9	3.2	9.6	8.6
200 ℃ 24 h	3092	5017	974	254	320	19.7	15.7	3.8	12.2	9.7
300 ℃ 24 h	2791	4752	973	255	314	18.6	15.1	3.8	10.9	8.9
300 ℃ 48 h	3099	4821	978	237	286	20.4	16.9	4.1	13.1	10.8
350 ℃ 24 h	2597	2272	526	87	79	26.1	28.7	6.0	30	33
385 ℃, 24 h	1820	1100	245	30	16	36.6	69.2	8.1	60	114
400 ℃, 12h	180.5	35.57	9.11	1.02	0.32	34.9	110	8.95	177	557
Batch 2, 385 ℃, varied reaction time, 1 mbar										
385 ℃ 1 h	2979	5100	1013	281	301	18.1	16.9	3.6	10.6	9.9
385 ℃ 2 h	2945	4532	943	213	243	21.3	18.6	4.4	14	12
385 ℃ 4 h	2525	3876	815	165	169	23.6	22.9	4.9	15	15
385 ℃ 8 h	2328	1956	445	72	58	27.1	34.0	6.2	32	40
385 ℃ 12 h	2204	1680	395	56	30	29.9	56.5	7.0	39	74
385 ℃ 24 h	1820	1100	245	30	16	36.6	69.2	8.1	60	114
Batch 3, varied vacuum pressure										
385 ℃, 1 mbar, 1 h	2979	5100	1013	281	301	18.1	16.9	3.6	11	10
385 ℃, 10 mbar, 1 h	2674	3716	730	154	148	24.2	25.0	4.8	17	18
385 ℃, 20 mbar, 1 h	2625	2968	584	108	102	27.4	29.2	5.4	24	26
385 ℃, 50 mbar, 1 h	2501	2474	485	79	63	31.3	39.4	6.1	32	40
385 ℃, 100 mbar, 1 h	2309	1794	376	57	41	31.4	43.3	6.6	40	56
385 ℃, 100 mbar, 2 h	1446	297	74	8.0	4.1	37.0	72.4	9.2	180	352
385 ℃ , 200 mbar, 20 min	1828	1460	313	54	45	26.8	32.2	5.7	34	40
385 ℃, 1 bar air, 10 min	1547	518	121	13.6	7.5	38.0	69.3	8.9	114	207
Batch 4, varied O_2 concentration										
385 ℃, Argon (O_2<10ppb) 1 h	3184	6470	1176	436	614	14.8	10.5	2.70	7.3	5.2
385 ℃, 10 ppm O_2/Ar, 1 h	3128	6068	1261	413	533	14.7	11.4	3.06	7.6	5.9
385 ℃, 50 ppm O_2/Ar, 1 h	2953	5223	1113	331	397	15.8	13.2	3.37	8.9	7.4
385 ℃, 100 ppm O_2/Ar, 1 h	2120	3781	746	210	261	18.0	14.5	3.54	10.1	8.1
385 ℃, 200 ppm O_2/Ar, 1 h	1450	2473	471	115	129	21.4	19.1	4.08	12.6	11.2
Batch 5, varied O_2 concentration										
385 ℃, Argon (O_2<10ppb), 24 h	2796	4468	907	232	213	19.3	21.0	3.9	12.1	13.1
385 ℃, 10 ppm O_2/Ar, 24 h	2768	3945	853	196	145	20.1	27.3	4.4	14.1	19.1
385 ℃, 50 ppm O_2/Ar, 24 h	2091	1902	439	76	48	24.9	39.6	5.8	27.4	43.5
385 ℃, 100 ppm O_2/Ar, 24 h	1955	1540	340	55	26	28.0	59.4	6.2	35.5	75.4

Supplementary Table 4. Representative gas transport properties of thermo-oxidatively crosslinked (TOX) PIM-1 membranes, thermally rearranged (TR) polymers, and carbon molecular sieve (CMS) membranes. 1 Barrer = 10^{-10} cm^3 (STP) cm cm^{-2} s^{-1} $cmHg^{-1}$.

Sample	Permeability (Barrer)					Selectivity					Ref
	H_2	CO_2	O_2	N_2	CH_4	CO_2/N_2	CO_2/CH_4	O_2/N_2	H_2/N_2	H_2/CH_4	
PIM-1 120°C vacuum 24 h	**3408**	**5135**	**1135**	**356**	**397**	**14.4**	**12.9**	**3.2**	**9.6**	**8.6**	This
TOX-PIM-1 385°C 1mbar 1 h	**2979**	**5100**	**1013**	**281**	**301**	**18**	**17**	**3.6**	**11**	**10**	This
TOX-PIM-1 385°C 1mbar 8 h	**2328**	**1956**	**445**	**72**	**58**	**27**	**34**	**6.2**	**32**	**40**	This
TOX-PIM-1 385°C 1mbar 12 h	**2204**	**1680**	**395**	**56**	**30**	**30**	**56**	**7.0**	**39**	**74**	This
TOX-PIM-1 385°C 1mbar 24 h	**1820**	**1104**	**245**	**30**	**16**	**37**	**69**	**8.1**	**60**	**114**	This
TOX-PIM-1 385°C 1mbar 24 h, 30 days	**1649**	**514**	**128**	**14.8**	**6.6**	**35**	**78**	**8.7**	**112**	**250**	This
TOX-PIM-1 385°C 1mbar 24 h, 455 days	**1380**	**310**	**70**	**8.10**	**4.06**	**38**	**76**	**8.6**	**170**	**340**	This
TOX-PIM-1 385°C argon 24 h	**2796**	**4468**	**907**	**232**	**213**	**19**	**21**	**3.9**	**12**	**13**	This
TOX-PIM-1 385°C 10ppm O_2 24 h	**2768**	**3945**	**853**	**196**	**145**	**20**	**27**	**4.4**	**14**	**19**	This
TOX-PIM-1 385°C 10ppm O_2 24 h, 30 days	**2139**	**1488**	**348**	**48**	**27**	**31**	**56**	**7.2**	**44**	**80**	This
TOX-PIM-1 385°C 10ppm O_2 24 h, 335 days	**1967**	**995**	**262**	**34.4**	**18.9**	**29**	**53**	**7.6**	**57**	**104**	This
TOX-PIM-1 385°C 100ppm O_2 24 h	**1955**	**1540**	**340**	**55**	**25.9**	**28**	**59**	**6.2**	**36**	**75**	This
TOX-PIM-1 385°C 100ppm O_2 24 h, 30 days	**1593**	**780**	**206**	**23.9**	**10.3**	**33**	**76**	**8.6**	**67**	**155**	This
TOX-PIM-1 385°C 100ppm O_2 24 h, 325 days	**944**	**365**	**105**	**10.9**	**4.77**	**33**	**77**	**9.6**	**87**	**198**	This
TOX-PIM-1 385°C air 10 min	**1547**	**518**	**121**	**13.6**	**7.5**	**38**	**69**	**8.9**	**114**	**207**	This
PIM-1 300°C 24h vacuum	2221	3083	483	101	91	30.7	34	4.8	22	25	6
PIM-1 300°C 48h vacuum	3872	4000	582	96	73	42	55	6.1	40	53	6
TZ-PIM-1		3076		101		30.5					7
TZ-PIM-2		2509		87		28.9					7
PIM-EA-TB	7760	7140	2150	525	699	13.6	10.2	4.1	14.8	11.1	2
PIM-SBI-TB	2200	2900	720	232	450	12.5	6.4	3.1	9.5	4.9	2
PIM-SBF	6320	13900	2640	786	1100	17.7	12.6	3.4	8.0	5.7	8
Crosslinked DC-PIM-1		2345	554	161	192	15	12	3.4			9
Crosslinked DC-PIM-5		1291	231	50	53	26	25	4.6			9
Crosslinked PIM-1/azide1(95:5)		3044	656	188		16.2		3.5			10
Crosslinked PIM-1/azide1 (80:20)		580	114	32		18.1		3.6			10
Crosslinked PIM-1/azide2 (95:5)		1606	315	71		22.6		4.4			10
Crosslinked PIM-1/azide2 (80:20)		219	38	8		27.4		4.8			10
TR-PBI	1779	1624	337	62	35	26	46	5.4	29	51	11
TRS		1591		75	47	21	34				4,12
TR-Polymer 1		1715		97	46	18	37				4,12
TR-Polymer 2		73		2.2	1.3	33	58				4,12
TR-Polymer 3		468		16	10	29	45				4,12
TR-Polymer 4		629		20	16	32	41				4,12
TR-Polymer 5		952		34	24	28	41				4,12
TR-Polymer 6		4134		164	122	25	34				4,12
tPBO	4194	4201	1092	284	151	15	28	3.8	15	28	13
aPBO	408	398	81	19	12	21	34	4.3	21	35	13
cPBO	3612	5568	1306	431	252	13	22	3.0	8	14	13
sPBO	3585	5903	1354	350	260	17	23	3.9	10	14	13
PBO-co-PPL 55 450°C	1989	1874	421	94	50	20	37	4.5	21	40	14
PBO-co-PPL 55 450°C	2895	1805	475	85	46	21	39	5.6	34	63	14
PBO-co-PPL 28 450°C	1680	525	132	18	6.7	29	78	7.3	93	251	14
spiroTR-PBO-6FDA 425°C	429	675	120	30	34	22.5	19.9	4.0	14.3	12.6	3
spiroTR-PBO-PM 425°C	261	263	48	11	15	23.9	17.5	4.4	23.7	17.4	3
PIM-6FDA-OH	259	251	45	11	9	23	28	4.1	24	28	15
PIM-6FDA-OH 440°C	578	683	150	43	50	16	14	3.5	13	12	15
PIM-6FDA-OH 530°C (CMS)	2860	4110	864	223	209	18	20	3.9	13	14	15
PIM-6FDA-OH 600°C (CMS)	5248	5040	1071	185	132	27	38	5.8	28	40	15
PIM-6FDA-OH 630°C (CMS)	4693	2871	839	123	58	23	50	6.8	38	81	15
PIM-6FDA-OH 800°C (CMS)	2177	556	149	17	6	33	93	8.8	128	363	15

Supplementary Table 4 continued

Sample	Permeability (Barrer)					Selectivity					Ref
	H_2	CO_2	O_2	N_2	CH_4	CO_2/N_2	CO_2/CH_4	O_2/N_2	H_2/N_2	H_2/CH_4	
Matrimid CMS 550°C		1250	435	50	20	25	63	8.7			16
Matrimid CMS 550°C		375	166	18.2	4.2	21	89	9.1			16
Matrimid CMS 800°C		43.5	24	1.8	0.21	24	200	13.3			16
Matrimid CMS 550°C		1264	323	42.5	19.4	30	65	7.6			17
Matrimid CMS 800°C		66	24	1.86	0.32	35	209	12.9			17
6FDA/BPDA-DAM CMS 550°C		4864	1052	148	90.1	33	54	7.1			17
6FDA/BPDA-DAM CMS 800°C		94	24	2.11	0.77	45	122	11.4			17
6FDA/BPDA-DAM CMS 550°C He		2845			53		54				18
6FDA/BPDA-DAM CMS 550°C Ar		3110			25		122				18
6FDA/BPDA-DAM CMS 550°C 0.005Torr		2580			36		71				18
6FDA/BPDA-DAM CMS 550°C 0.042Torr		240			2		110				18
6FDA/BPDA-DAM CMS 550°C vacuum		~3100			39		~80				18
6FDA/BPDA-DAM CMS 550°C 4ppm O_2		~7000			226		~31				18
6FDA/BPDA-DAM CMS 550°C 8ppm O_2		~4800			87		~55				18
6FDA/BPDA-DAM CMS 550°C 30 ppm O_2		~2330			35		~67				18
6FDA/BPDA-DAM CMS 550°C 50 ppm O_2		~530			23		~23				18
6FDA/PMDA–TMMDA CMS 550°C		1300	418	77	45	17	29	5.4			19
6FDA/PMDA–TMMDA CMS 650°C		751	259	39	21	19	36	6.6			19
6FDA/PMDA–TMMDA CMS 800°C		519	184	18	5.4	29	96	10.2			19

Note CMS membranes are listed only for comparison of the gas separation data, while in fact our TOX PIM membranes are essentially still in polymeric state.

Supplementary Note 1: Apparent reaction kinetics of thermal oxidation of PIM-1 polymer

From the viewpoint of chemical reaction engineering, the thermal oxidative crosslinking or degradation of PIM-1 polymer could be influenced by a variety of parameters, such as heat transfer (conduction and convection), external mass transfer (diffusion of oxygen from bulk to the surface), chemical reaction (oxidative chain scission and crosslinking, and also probably decomposition), and change of internal diffusion (diffusion of oxygen and products in polymer matrix) due to complicated physical and chemical changes (local change of micropore structure). In this study, the reaction rate was not limited by external mass transfer given sufficient gas flow rate. Owing to the high O_2 permeability (~1000 Barrer) and particularly high diffusion coefficient of oxygen, internal diffusion is not limiting the reactions as proved by samples with different thickness. Over the reaction temperature range (<400 ℃), thermal decomposition could be assumed as not so significant compared to oxidative crosslinking. Therefore, the thermal degradation of PIM-1 polymer film is likely to be kinetically controlled by gas-solid chemical reactions of polymer with oxygen, and can be described as the following equation:

$$\frac{dw}{dt} = r = k_0 \exp(-\frac{E_a}{RT})(C_{O_2,b} - C_{O_2,e})^n \quad (6)$$

where dw/dt and r is the rate of reaction, k_0 is the coefficient of rate constant, E_a is the apparent activation energy, R is gas constant, T is temperature, $C_{O_2,e}$ is the equilibrium concentration of O_2 in the polymer matrix, $C_{O_2,b}$ is the bulk concentration. Therefore, the degree of oxidation and crosslinking of polymer could be tuned by controlling the parameters, such as the temperature, oxygen concentration, and time.

The equilibrium oxygen concentration is subject to chemisorption at the reaction temperature:

$$C_{O_2,e} = k_D P_{O_2} + \frac{C_H' b P_{O_2}}{1 + b P_{O_2}} \quad (7)$$

Assuming the difference between the equilibrium and the bulk concentration as constant, the apparent activation energy could be derived.

Alternatively, the TGA was operated in modulated mode and the activation energy derived from high-resolution dynamic heating protocol gave similar values of activation energy.

Supplementary Methods

Single gas permeation

Pure gas permeation tests were carried out at temperature of 22 ℃ and feed pressure of 4 bar, using a constant-volume pressure-increase apparatus described elsewhere[20]. A piece of membrane was loaded in the apparatus and thoroughly evacuated with a vacuum pump (Edwards RV3) prior to gas permeation measurements. The leak rate is negligible with good sealing and evacuation. The gas permeate pressure were continuously recorded by pressure transmitters (Keller PAA 33X, Accuracy of 0.01% F.S.) connected to a data acquisition system. When the gas permeation reached to pseudo-steady state, the slope of pressure increase (dp/dt) in the permeate chamber became constant. The constant slope could be verified by evacuating the downstream briefly and measuring the increase of permeate pressure again.

The gas permeability (P) is calculated based on the following equation:

$$P = \frac{Vl}{A}\frac{T_0}{p_f p_0 T}\left(\frac{dp}{dt}\right) \quad (1)$$

where P is the permeability of the gas through the membrane, expressed in Barrer (1 Barrer=10^{-10} cm^3(STP)cm cm^{-2} s^{-1} $cmHg^{-1}$), V is the permeate volume (cm^3), l is the thickness of membrane (cm), A is the effective area of the membrane (2.2 or 12.6 cm^2), p_f is the feed pressure (cmHg), p_0 is the pressure at standard state (76 cmHg), T is the absolute operating temperature (K), T_0 is the temperature at standard state (273.15 K), (dp/dt) is the slope of pressure increase in the permeate volume at pseudo-steady state (cmHg s^{-1}). The error of the calculated permeability mainly originated from the variation of membrane thickness; for this study, the uncertainties of gas permeability at the moment of test are within ±5%, and selectivity within ±7%.

The diffusion coefficient (D) for a specific gas can be derived from the thickness of the membrane and the time lag (θ):

$$D = \frac{l^2}{6\theta} \quad (2)$$

Then the solubility (S) can be derived from:

$$S = \frac{P}{D} \quad (3)$$

Alternatively, the solubility is derived from the gas sorption measurements at 1 bar, and the diffusion co-efficient (at 1 bar) is calculated from the permeability (D=P/S), because the gas permeability is constant over the low pressure range. This was later verified by gas permeation at 1 bar.

The ideal selectivity ($\alpha_{A/B}$) of gas pairs, A and B, is defined as:

$$\alpha_{A/B} = \frac{P_A}{P_B} = \left[\frac{D_A}{D_B}\right]\left[\frac{S_A}{S_B}\right] \quad (4)$$

where D_A/D_B is the diffusivity selectivity and S_A/S_B is the solubility selectivity.

Mixed gas permeation

The mixed gas permeation properties were measured in another membrane cell using the constant-pressure variable-volume method. The membrane was exposed to certified gas mixtures (BOC, UK) of CO_2/CH_4 (50/50 vol.%) and CO_2/N_2 (50/50 vol.%) with feed pressure up to 35 bar at room temperature (22 ℃), with a stage cut (ratio of flow rates of permeate to feed) less than 1 %. The feed flow rate was controlled by a metering valve (Swagelok) and measured by a flow meter (Aldrich). The flow rate of permeate was measured using a soap bubble flow meter (Aldrich). The compositions of feed and permeate gas mixtures were measured by a gas chromatograph (Shimadzu, model 2014) equipped with a thermal conductivity detector (TCD) and a flame ionization detector (FID) calibrated by certified gas mixtures (Scientific and Technical Gases LTD, UK). By measuring the permeate flow rate (Q_P) and gas compositions with GC, the

permeability of the gas specie *i* through the membrane, P_i (Barrer, 1 Barrer=1×10^{-10} cm^3 (STP) cm cm^{-2} s^{-1} $cmHg^{-1}$), is calculated as:

$$P_i = \frac{Q_p x_{p,i} l}{A(p_f x_{f,i} - p_p x_{p,i})} \quad (5)$$

Where $x_{p,i}$ is the volume fraction of component *i* in the permeate gas; $x_{f,i}$ is the volume fraction of species *i* in the feed gas; *A* is the effective area of membrane (cm^2); *l* is the thickness of membrane (cm); p_f is the feed pressure (cmHg); p_p is the permeate pressure (cmHg). In some experiments, when the permeate flow rate was too low to be accurately measured by the soap bubble flow meter, carrier gas (Helium) was used to sweep the permeate gas with flow rate controlled by a mass flow controller (Bronkhorst Ltd, model EL flow). With the permeability of each species, the selectivity is calculated from $\alpha_{A/B} = P_A / P_B$.

Supplementary References

1. Song, J. *et al.*, Linear high molecular weight ladder polymers by optimized polycondensation of tetrahydroxytetramethylspirobisindane and 1,4-dicyanotetrafluorobenzene. *Macromolecules* **41**, 7411-7417 (2008).
2. Carta, M. *et al.*, An Efficient Polymer Molecular Sieve for Membrane Gas Separations. *Science* **339**, 303-307 (2013).
3. Li, S. *et al.*, Mechanically robust thermally rearranged (TR) polymer membranes with spirobisindane for gas separation. *J. Membr. Sci.* **434**, 137-147 (2013).
4. Park, H. B. *et al.*, Polymers with Cavities Tuned for Fast Selective Transport of Small Molecules and Ions. *Science* **318**, 254-258 (2007).
5. Teplyakov, V. & Meares, P., Correlation aspects of the selective gas permeabilities of polymeric materials and membranes. *Gas Separation & Purification* **4**, 66-74 (1990).
6. Li, F. Y., Xiao, Y., Chung, T.-S., & Kawi, S., High-Performance Thermally Self-Cross-Linked Polymer of Intrinsic Microporosity (PIM-1) Membranes for Energy Development. *Macromolecules* **45**, 1427-1437 (2012).
7. Du, N. *et al.*, Polymer nanosieve membranes for CO2-capture applications. *Nat. Mater.* **10**, 372-375 (2011).
8. Bezzu, C. G. *et al.*, A Spirobifluorene-Based Polymer of Intrinsic Microporosity with Improved Performance for Gas Separation. *Adv. Mater.* **24**, 5930-5933 (2012).
9. Du, N., Dal-Cin, M. M., Robertson, G. P., & Guiver, M. D., Decarboxylation-Induced Cross-Linking of Polymers of Intrinsic Microporosity (PIMs) for Membrane Gas Separation. *Macromolecules* **45**, 5134-5139 (2012).
10. Du, N. *et al.*, Azide-based Cross-Linking of Polymers of Intrinsic Microporosity (PIMs) for Condensable Gas Separation. *Macromol. Rapid Commun.* **32**, 631-636 (2011).
11. Han, S. H. *et al.*, Highly gas permeable and microporous polybenzimidazole membrane by thermal rearrangement. *J. Membr. Sci.* **357**, 143-151 (2010).
12. Park, H. B. *et al.*, Thermally rearranged (TR) polymer membranes for CO_2 separation. *J. Membr. Sci.* **359**, 11-24 (2010).
13. Han, S. H. *et al.*, Thermally Rearranged (TR) Polybenzoxazole: Effects of Diverse Imidization Routes on Physical Properties and Gas Transport Behaviors. *Macromolecules* **43**, 7657-7667 (2010).
14. Choi, J. I. *et al.*, Thermally rearranged (TR) poly(benzoxazole-co-pyrrolone) membranes tuned for high gas permeability and selectivity. *J. Membr. Sci.* **349**, 358-368 (2010).
15. Ma, X. *et al.*, Carbon molecular sieve gas separation membranes based on an intrinsically microporous polyimide precursor. *Carbon* **62**, 88-96 (2013).
16. Vu, D. Q., Koros, W. J., & Miller, S. J., Mixed matrix membranes using carbon molecular sieves - I. Preparation and experimental results. *J. Membr. Sci.* **211**, 311-334 (2003).
17. Steel, K. M. & Koros, W. J., An investigation of the effects of pyrolysis parameters on gas separation properties of carbon materials. *Carbon* **43**, 1843-1856 (2005).
18. Kiyono, M., Williams, P. J., & Koros, W. J., Effect of pyrolysis atmosphere on separation performance of carbon molecular sieve membranes. *J. Membr. Sci.* **359**, 2-10 (2010).
19. Shao, L. *et al.*, Casting solvent effects on morphologies, gas transport properties of a novel 6FDA/PMDA-TMMDA copolyimide membrane and its derived carbon membranes. *J. Membr. Sci.* **244**, 77-87 (2004).
20. Song, Q. *et al.*, Zeolitic imidazolate framework (ZIF-8) based polymer nanocomposite membranes for gas separation. *Energy Environ. Sci.* **5**, 8359-8369 (2012).